THE ASTROPHYSICAL JOURNAL, 334:665–687, 1988 November 15

SPECTRAL SYNTHESIS IN THE ULTRAVIOLET. II. STELLAR POPULATIONS AND STAR FORMATION IN BLUE COMPACT GALAXIES[1]

MICHAEL N. FANELLI, ROBERT W. O'CONNELL, AND TRINH X. THUAN
Astronomy Department, University of Virginia
Received 1988 March 14; accepted 1988 May 12

ABSTRACT

Far-UV spectra of seven blue compact galaxies have been obtained with the *IUE* satellite. These objects span a range in luminosity of $-21 \leq M_B \leq -13$. We have investigated their stellar content and star formation history by applying the technique of optimizing population synthesis utilizing the library of far-UV stellar spectra developed by Fanelli, O'Connell, and Thuan.

The far-UV absorption-line spectra of these galaxies are clearly composite, with the signatures of main-sequence types between O3 and mid-A. Most of the low-ionization absorption lines have a stellar origin. The Si IV and C IV features in several objects have P Cygni profiles. In Haro 1 the strength of Si IV indicates a significant blue supergiant population. The metal-poor blue compact dwarf Mrk 209 displays weak absorption lines, evidence that the stellar component has the same low metallicity as observed in the ionized gas ($Z \approx 0.1\ Z_\odot$).

Good fits to the data are obtained with the synthesis technique. We find that the solutions yield stellar luminosity functions which display large discontinuities, indicative of discrete star formation episodes or bursts. Continuous star formation cannot account for the observations. The current burst of star formation appears to have lasted for less than 10 Myr. In all cases except Mrk 209 there is evidence of earlier star formation episodes. For Haro 2 there were at least two earlier bursts, the most recent of which ended not more than $\sim$20 Myr ago. The A star populations in our models point to significant star formation activity 500 Myr or more ago. In the cases other than that of Haro 2, we cannot distinguish between a few isolated bursts and a continuing series of short bursts separated by $\sim$20–30 Myr.

The amount of UV extinction is found to be low, $0.0 \lesssim E(B-V) \lesssim 0.35$, significantly smaller than values derived from the Balmer decrement for the same object. The UV light preferentially emerges through windows of low optical depth. We find evidence for a positive correlation between the amount of UV extinction and the metallicity of the galaxy.

UV synthesis provides an independent estimate of the current ionizing star content which appears to be in agreement with estimates based on observations in the visible, radio, and infrared. Star formation rates can also be estimated for the hot stars detected directly in the UV, and these rates highlight the intensity of the starbursts. In the more luminous galaxies Haro 1 and Haro 15, $\sim 3\ M_\odot\ \mathrm{yr}^{-1}$ of gas is being converted into massive ($m \gtrsim 10\ M_\odot$) stars, a value independent of the nature of the initial mass function.

Subject headings: galaxies: stellar content — stars: formation — ultraviolet: spectra

I. INTRODUCTION

Blue compact galaxies (BCGs) are now recognized to be extragalactic systems where intense bursts of star formation are occurring. Before the launch of the *International Ultraviolet Explorer* (*IUE*) satellite, the observational evidence for active star formation rested mainly on optical data. BCGs have very blue *UBV* colors, and their optical spectra show strong, narrow emission lines superposed on a nearly featureless continuum, similar to the spectrum of H II regions, implying the presence of many young, ionizing OB stars (Searle and Sargent 1972; Searle, Sargent, and Bagnuolo 1973; Huchra 1977*a*, *b*; O'Connell, Thuan, and Goldstein 1978; Lequeux *et al.* 1979; French 1980; Kinman and Davidson 1981; Viallefond and Thuan 1983, hereafter VT83; Kunth and Sargent 1983). These authors argue that star formation in BCGs cannot be continuous but must proceed in bursts because the current rate of star formation would produce more metals than observed (most BCGs are metal-deficient, with $0.03 \lesssim Z/Z_\odot \lesssim 0.5$) in $\sim 10^8$ yr, and exhaust the gas supply in $\sim 10^9$ yr. More recent data, especially those from the *IRAS* mission, have indicated that these intense star formation episodes, now popularly referred to as "starbursts," are more common than previously realized. Starbursts can occur in interacting galaxies (Gehrz, Sramek, and Weedman 1983), isolated systems (Tully *et al.* 1981; VT83; Bergvall 1985), galactic nuclei (Weedman *et al.* 1981; Balzano 1983), and high-redshift radio galaxies (Thuan and Condon 1987). A recent review of the starburst phenomenon in different environments and as a function of redshift can be found in Thuan, Montmerle, and Van (1988).

As a result of the energy output from massive stars, star-forming regions radiate strongly over much of the electromagnetic spectrum, providing a wealth of diagnostics to study intrinsic physical conditions. With *IUE*, ultraviolet spectra can be obtained which *directly* probe the massive star population in these objects. Moreover, the availability of the *IUE Spectral Atlas* (Wu *et al.* 1983), which contains ultraviolet spectra of stars spanning spectral types O3–M4 and is fairly complete regarding spectral type and luminosity class coverage, can be used in the application of spectral synthesis techniques to

[1] Based on observations obtained with the *International Ultraviolet Explorer* satellite, which is sponsored and operated by the United States National Aeronautics and Space Administration, by the Science Research Council of the United Kingdom, and by the European Space Agency.

ultraviolet spectra (Fanelli, O'Connell, and Thuan 1987, hereafter Paper I). The distribution of stars in various evolutionary stages (main-sequence, giant, supergiant) which best fits the observed spectral energy distribution can be derived. The current stellar luminosity function can also be estimated and provides valuable information on the past history of star formation.

In this paper, we present an initial attempt to apply optimizing spectral synthesis techniques to the far-UV spectra of BCGs. This approach is complementary to the evolutionary synthesis method, in which the time evolution of a composite spectral energy distribution (SED) is calculated assuming a specific set of parameters (initial mass function, star formation rate, and stellar evolutionary tracks). Section II is a general discussion of the far-UV properties of star-forming regions. In § III we describe our *IUE* observations. In § IV we detail the optimizing synthesis technique. We present the synthesis results in § V, discuss the ultraviolet and optical extinction in § VI, and examine the nature of the absorption-line component in § VII. The stellar content and star formation history are discussed in § VIII, the evolved stellar population in § IX, and the ionizing stellar population in § X. Section XI is a summary of our conclusions. Some of these results have been presented in a preliminary form by Thuan (1986, 1988).

II. INTERPRETATION OF THE ULTRAVIOLET SPECTRA OF STAR-FORMING REGIONS

The far-ultraviolet wavelength region offers new opportunities but also presents many new challenges in the study of star-forming regions. The emergent SED is a mixture of the integrated light of the stellar population and the effects of interstellar gas and dust. The stellar component is the sum of all spectral types and luminosity classes which produce appreciable flux in the far-UV. Until recently, it was anticipated that the far-UV stellar SED would arise almost exclusively from main-sequence stars of spectral types O–A, since early stellar evolutionary models predicted that massive stars evolve rapidly with roughly constant luminosity to the red supergiant phase after core hydrogen exhaustion (Iben 1967; Clayton 1968; Stothers and Chin 1976), and the far-UV flux becomes negligible for stars with spectral types later than ~F0. The time spent in a hot main-sequence phase was estimated to be more than 90% of the total stellar lifetime. More recent investigations cast doubt on these simple models. Comparison of model calculations of massive stars with composite (cluster and field) H-R diagrams indicates that many more post–main-sequence stars (as defined by spectral line criteria) are observed than predicted. It appears that young, massive stars can still be in the core hydrogen-burning phase while exhibiting OBAF giant and supergiant characteristics, an effect termed "main-sequence widening" (Meylan and Maeder 1982; Humphreys and McElroy 1984; Bertelli, Bressan, and Chiosi 1984).

This observed distribution of stars in the upper H-R diagram is apparently due to the interplay of several poorly understood physical effects, including mass loss during main-sequence and post–main-sequence evolution, semiconvective instability, and convective overshoot (see Chiosi and Maeder 1986 for a recent review). Evolutionary models incorporating these effects produce a variety of tracks, some of which show little or no redward evolution while others loop back to the blue during the core helium-burning phase (Doom 1982; Maeder 1984; Chiosi and Maeder 1986). Therefore, the blue supergiant population may be a mixture of *both* hydrogen- and helium-burning phases. Massive stars can apparently end their evolution as blue supergiants, as evidenced by SN 1987A, whose progenitor was identified as a B3 Ia supergiant (West, Lauberts, and Schuster 1987). The metallicity of the stellar population may also affect the relative lifetimes of evolutionary phases. Theoretical tracks (Brunish and Truran 1982*a*, *b*) for low-metallicity massive stars show a trend for diminished redward evolution as the metal abundance decreases. This additional effect may be important in BCGs, many of which have low gas-phase abundances (Matteucci and Chiosi 1983). Additionally, spectral features characteristic of Wolf-Rayet stars, which are highly evolved massive stars (Chiosi 1982; Conti *et al.* 1983; Humphreys, Nichols, and Massey 1985), are observed in some extragalactic H II regions (Osterbrock and Cohen 1982; Massey and Conti 1983; Kunth and Schild 1986).

Taken together, these results indicate that *the post–main-sequence lifetimes of massive stars are longer than originally predicted, that some of this evolutionary phase may be spent in a UV-luminous* ($T > 7500$ K) *state and that current theoretical models for the evolution of massive stars do not seem capable of adequately predicting the lifetimes of various evolutionary phases.* This is a serious complication for any analysis of stellar populations through integrated light, although optimizing synthesis, which need make no assumptions regarding the expected stellar evolutionary rates, can be less affected than other approaches.

The interstellar and circumstellar medium affects the ultraviolet SED in several ways. For example, C IV λ1550 can arise as both an absorption and an emission feature in the stellar photosphere and wind of an O star, as an emission line in H II regions surrounding very hot stars, and as an absorption feature in interstellar coronal gas. C IV λ1550, Si IV $\lambda\lambda$1394, 1403, N V λ1240, and occasionally N IV λ1719 show P Cygni profiles (blueshifted and widened absorption feature with redshifted emission) as a result of circumstellar winds in O and early B stars. Foreground Galactic line absorption can also affect the spectra of star-forming regions; for the low-resolution (6 Å) mode of *IUE*, objects must be redshifted by about 10 Å (2000 km s^{-1}) for clear separation of local from intrinsic absorption-line components.

The entire spectral energy distribution is further affected by general interstellar extinction caused by dust along the line of sight. While the Galactic component will be small for objects at high latitude, intrinsic extinction can have a major effect on the source SED. Unfortunately, the ultraviolet reddening law, which has been extensively studied with *IUE* data, shows marked nonuniformities from place to place in the Galaxy (Massa, Savage, and Fitzpatrick 1983; Witt, Bohlin, and Stecher 1984; Massa and Fitzpatrick 1986) and may not be subject to simple parameterization. There is evidence for variations from galaxy to galaxy. Extinction laws for the LMC (Nandy *et al.* 1980) and the SMC (Rocca-Volmerange *et al.* 1981) are steeper at shorter wavelengths than the Galactic law (Savage and Mathis 1979).

Compounding this uncertainty in the wavelength dependence of the extinction law are the effects of scattering and geometry in star-forming complexes. Many of the emergent photons from such regions are expected to have been scattered at least once by dust grains (e.g., Bohlin *et al.* 1982). Furthermore, one expects that only the least obscured regions will make major contributions to the emergent UV flux, implying

that *one may be sampling different parts of the complex in the UV and visible.* Given the nature of the data in hand, there is no realistic way in which one could model such effects. Therefore, we have treated the data as though there were a simple absorbing screen between the telescope and the stars with a wavelength-dependent opacity given by the Savage and Mathis (1979) law. We shall test for scattering-dominated spectra in the synthesis by using negative values for the intrinsic color excess.

Interstellar emission can also affect the SED, though not strongly. Nebular continuum emission is not expected to be important in the UV (Israel and Koornneef 1979; Lequeux *et al.* 1981). In addition to C IV λ1550, emission lines of N IV] λ1486, O III] λ1666, and C III] λ1909 may be present but will be difficult to detect owing to low contrast against the strong continuum (Dufour, Shields, and Talbot 1982). These lines are more frequently observed in the lower luminosity, high-excitation blue compact dwarfs.

Despite the uncertainties caused by general obscuration and potential interstellar absorption-line contamination, we are optimistic that ultraviolet spectral synthesis can provide tangible results. The primary advantage is the suppression of cool starlight in the far-UV. At optical and near-infrared wavelengths most spectral types contribute to the integrated light, both from the burst component and from any underlying cooler population (regardless of its age). But for $\lambda < 1900$ Å only stars with spectral types earlier than ~A7 ($T \geq 7500$ K) produce appreciable flux. The presence of cooler stars in astrophysically reasonable numbers will not be detectable and will not complicate an attempt to model the hot star population. Two additional factors weigh in our favor: (1) many strong absorption lines are seen in far-UV spectra (Paper I) which will facilitate the determination of the stellar content, and (2) the strong, blue continua which define BCGs imply that the overall extinction should be relatively small.

III. ULTRAVIOLET OBSERVATIONS

a) Observations and Data Reduction

The BCGs discussed in this paper were selected from the compilation of Thuan and Martin (1981), who listed all known such galaxies from the Markarian (1967) (Mrk), Haro (1956), and Zwicky and Zwicky (1971) (Zw) catalogs up to 1980. In order to maximize the signal-to-noise ratio in the ultraviolet, the candidate BCGs were chosen to be bright in total blue apparent magnitude, $B_T \leq 14.5$; to have blue colors, ($B-V \lesssim 0.5$ and $U-B \lesssim -0.2$); and to be at high Galactic latitude, $b \gtrsim 25°$, in order to avoid Galactic extinction. Two of the program galaxies, Mrk 209 and VII Zw 403, are dwarfs with $M_B \gtrsim -17$. Three (Haro 2, Haro 3, and Mrk 86) are of intermediate luminosity, $-17 \gtrsim M_B \gtrsim -19$. We also included two objects, Haro 1 and Haro 15, which exhibit similar morphological characteristics but are about 2 mag brighter, $M_B \approx -21$. These galaxies were chosen to study the continuity of ultraviolet spectral properties of BCGs over a range of intrinsic luminosities. Basic data for the seven program galaxies are given in Table 1.

The data were obtained with the *IUE* in four 8 hr low-background shifts and two 8 hr high-background shifts. Only short-wavelength ($\lambda\lambda$1200–1950) spectra were obtained, because of time and signal-to-noise constraints. The log of our *IUE* observations is given in Table 2. All spectra were obtained with the large aperture (10″ × 20″) in the low-dispersion mode, giving a spectral resolution of about 6 Å. The aperture was centered visually on the brightest region of each BCG at the coordinates listed in Table 2. For Mrk 209 and Mrk 86, two separate exposures were taken with small declination offsets, but a careful examination did not reveal any appreciable difference between the individual spectra, and they were added together weighted by the integration times. Perpendicular to the dispersion direction, there are 10 spatially resolved gross

TABLE 1

GALAXY PROPERTIES

Object (1)	m_B (2)	$(B-V)_T^0$ (3)	r_{25} (4)	b/a (5)	V_0 (6)	D (7)	M_B (8)	d (9)	$a \times b$ (10)	M_H (11)	L_B (12)	M_H/L_B (13)	$E(B-V)_G$ (14)
Haro 1	12.77	0.32	61	1.00	3778	50.0	−21.2	14.9	2.4 × 4.8	6.0×10^9	4.7×10^{10}	0.13	0.12
Haro 2	13.17	0.36	67	0.95	1534	20.5	−18.5	6.6	1.0 × 2.0	4.6×10^8	3.8×10^9	0.12	0.02
Haro 3	13.15	0.47	89	0.74	1025	13.9	−17.6	5.9	0.6 × 1.3	5.4×10^8	1.9×10^9	0.28	0.02
Haro 15	13.88	0.20	69	0.72	6471	85.0	−21.1	29.0	4.0 × 8.0	5.5×10^9	4.3×10^{10}	0.13	0.08
Mrk 209	14.84	0.51	52	0.89	345	4.6	−14.0	1.2	0.2 × 0.4	4.1×10^7	4.3×10^7	0.95	0.03
Mrk 86	12.55	0.49	100	0.91	449	7.0	−17.1	3.4	0.7 × 0.3	2.4×10^8	1.1×10^9	0.22	0.11
VII Zw 403	14.77	0.38	100	0.60	111	3.2	−13.1	1.6	0.15 × 0.3	3.8×10^7	2.7×10^7	1.41	0.08

Col. (1).—Galaxy identification.

Col. (2).—Apparent (uncorrected) magnitude in the B system within a diameter corresponding to a surface brightness level of 25 mag arcsec^{-2}. These were taken from Thuan and Martin 1981 or derived from Longo and de Vaucouleurs 1983.

Col. (3).—$B-V$ color corrected for Galactic extinction using the color excess derived from Heiles 1975.

Col. (4).—Diameter in arcminutes at a surface brightness level of 25 mag arcsec^{-2} from de Vaucouleurs, de Vaucouleurs, and Corwin 1976 (hereafter RC2).

Col. (5).—Ratio of minor to major axis, from the RC2.

Col. (6).—Recession velocity taken from the centroid of the H I line profile corrected to the Local Group (Thuan and Martin 1981; Gordon and Gottesman 1981).

Col. (7).—Distance in megaparsecs determined from col. (6) and a Hubble constant of 75 km s^{-1} Mpc^{-1}. VII Zw 403 is assumed to belong to the M81 group.

Col. (8).—Absolute blue magnitude derived from m_B corrected for Galactic extinction and the distances in col. (7).

Col. (9).—Linear diameter in kiloparsecs corresponding to the angular diameter in col. (4) for the given distance.

Col. (10).—Linear diameter in kiloparsecs as observed through the *IUE* spectrograph aperture.

Col. (11).—Neutral hydrogen mass in solar units taken from Thuan and Martin 1981 or Gordon and Gottesman 1981. The corrected value adopted in VT83 has been used for Mrk 209.

Col. (12).—Blue luminosity in solar units derived from M_B and adopting $M_B(\odot) = 5.48$.

Col. (13).—Ratio of neutral hydrogen mass to blue light.

Col. (14).—Color excess due to Galactic extinction taken from Heiles 1975.

TABLE 2

OBSERVING LOG

Object[a] (1)	α (1950) (2)	δ (1950) (3)	b (4)	Image Number[b] (5)	Exposure Time (minutes) (6)	Date (7)
Haro 1	$07^h33^m39^s.4$	35°21′15″	24.0	11269	200	1981 Feb 8
Haro 2	10 29 22.5	54 39 30	52.8	10471	215	1980 Oct 25
Haro 3	10 42 16.4	56 13 20	53.4	10483	240	1980 Oct 26
Haro 15	00 46 04.0	−12 59 25	−75.6	11259	410	1981 Feb 7
Mrk 209	12 23 50.6	48 46 15	68.1	10495	407	1980 Oct 28
	12 23 50.6	48 46 07	...	10484	147	1980 Oct 27
Mrk 86	08 09 43.2	46 08 36	33.0	11270	165	1981 Feb 8
	08 09 43.1	46 08 33	...	10473	95	1980 Oct 25
VII Zw 403	11 24 36.9	79 15 58	37.3	10470	360	1980 Oct 24

[a] Haro 2 ≡ Mrk 33; Haro 3 ≡ Mrk 35; Mrk 209 ≡ I Zw 36.
[b] All images taken with SWP camera.

spectra (SRGS), each 2″.1 wide. Examination of the SRGS at the *IUE* Regional Data Analysis Facility of the Goddard Space Flight Center permits determination of the ultraviolet luminosity profile and the combination of SRGS which maximizes the signal-to-noise characteristics in each spectrum. Figure 1 shows the observed spectra in absolute energy units (Bohlin and Holm 1980) smoothed over three pixels to remove high-frequency noise. The overall photometric accuracy of *IUE* including calibration errors is estimated to be around 10% (Bohlin *et al.* 1980). Table 3 gives the observed SEDs corrected for redshift at the set of wavelengths adopted for spectral synthesis as defined in Paper I. Each entry is the mean flux in a 20 Å bandpass converted to a magnitude, and normalized to 1510 Å. No reddening correction is applied. We also give in Table 3 monochromatic luminosities at 1510 Å, also uncorrected for reddening. All spectra except those for Mrk 86 and VII Zw 403 are well exposed. As a measure of the quality of the data, we have determined the standard error of the mean flux averaged over all 18 ultraviolet bandpasses, ϵ_{obs}. This quantity is also given in Table 3.

Other examples of *IUE* spectra of star-forming regions have been published by Benvenuti, Casini, and Heidmann (1979, 1982*a*, *b*), Huchra *et al.* (1983), Fabbiano and Panagia (1983), and Lamb *et al.* (1985). Rosa, Joubert, and Benvenuti (1984) have published an atlas of *IUE* spectra of extragalactic H II regions.

b) Spectral Chacteristics

The spectra in Figure 1 display flat or blueward-rising continua and absorption lines of both high- and low-ionization

TABLE 3

ULTRAVIOLET ENERGY DISTRIBUTIONS[a]

λ (Å)	Haro 1	Haro 2	Haro 3	Haro 15	Mrk 209	VII Zw 403	Mrk 86
1240	0.29	−0.28	−0.11	−0.22	−0.44	0.25	−0.31
1280	−0.05	−0.47	−0.26	−0.25	−0.43	0.04	−0.03
1305	0.25	−0.25	−0.07	−0.02	−0.23	0.15	0.44
1355	0.05	−0.30	−0.05	−0.17	−0.21	0.12	0.16
1397	0.31	0.09	0.09	0.14	−0.12	0.15	−0.03
1425	0.05	−0.12	0.01	−0.04	−0.10	0.44	−0.26
1450	−0.16	−0.03	−0.01	−0.27	0.10	0.44	0.21
1485	−0.15	−0.11	−0.10	−0.19	−0.13	0.07	−0.51
1510	0.00	0.00	0.00	0.00	0.00	0.00	0.00
1539	0.46	0.39	0.27	0.29	0.13	0.18	0.10
1550	0.39	0.10	−0.14	0.27	−0.01	0.44	−0.42
1561	0.15	−0.03	−0.20	0.03	0.02	0.45	−0.37
1590	0.14	0.26	0.16	0.11	0.12	0.18	0.21
1620	0.27	0.19	0.26	0.14	0.35	0.66	0.66
1680	0.06	0.07	0.25	0.15	0.44	0.49	−0.28
1710	0.11	0.13	0.22	0.09	0.39	0.83	0.34
1813	0.20	0.10	0.32	0.22	0.50	0.60	0.09
1855	0.22	0.40	0.49	0.32	0.67	0.64	0.29
ϵ_{obs}[b]	3.4	3.7	3.1	2.9	3.3	7.0	11.0
F_λ[c]	2.65	4.33	4.22	2.07	2.22	1.15	0.87
L_λ[d]	79.3	21.8	9.75	179	0.56	0.14	0.51

[a] Normalized spectral energy distribution: $m_\lambda = -2.5 \times \log (F_\lambda/F_{1510})$. F_λ is the mean flux within a 20 Å bandwidth centered on the listed wavelength.
[b] Percentage error of the mean flux in each bandpass averaged over all 18 bandpasses.
[c] Observed monochromatic flux at 1510 Å in units of 10^{-14} ergs s^{-1} cm^{-2} Å^{-1}.
[d] Intrinsic monochromatic luminosity at 1510 Å in units of 10^{38} ergs s^{-1} Å^{-1}. No corrections for interstellar extinction have been made.

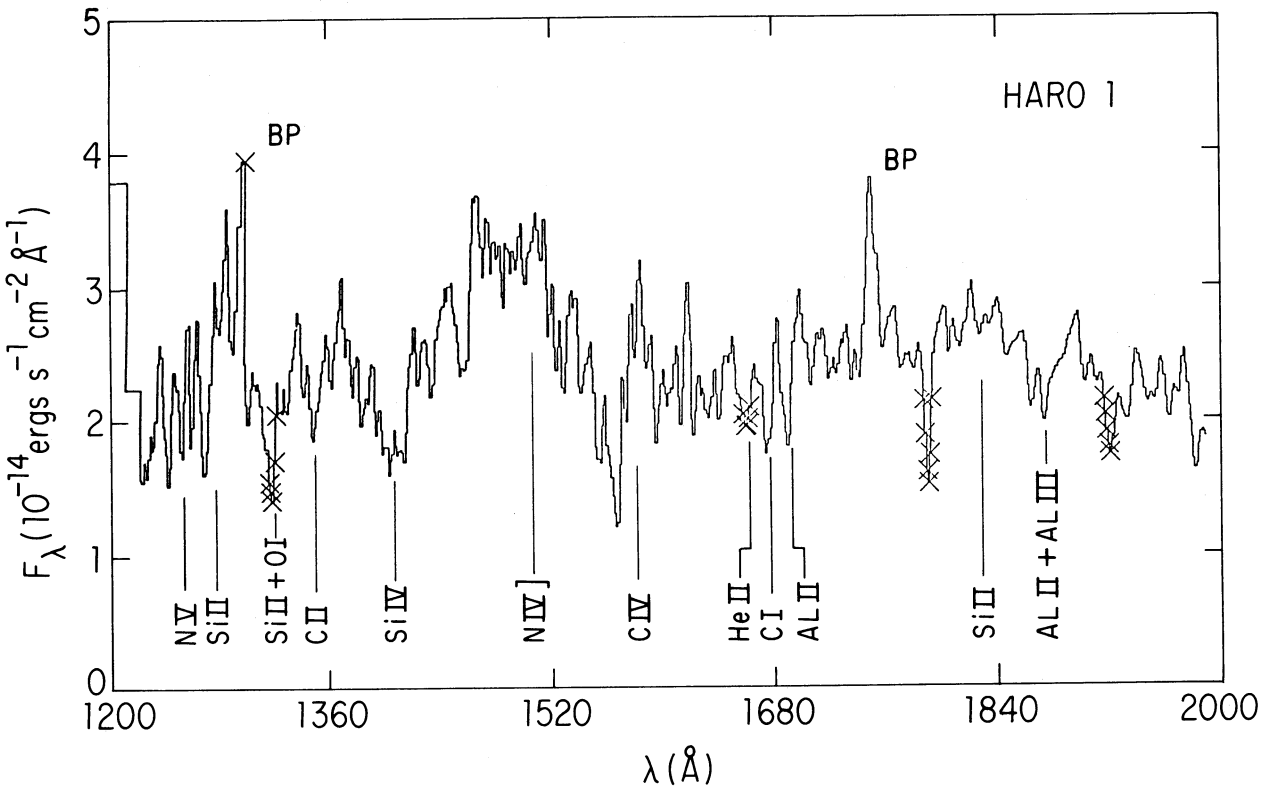

FIG. 1.—Far-UV spectra of seven blue compact galaxies observed with *IUE*. The spectra were individually extracted and smoothed with a 3-point boxcar filter. No correction for extinction or redshift has been applied. Principal line features in this spectral range are indicated. Crosses indicate the fiducial reseau marks placed on the *IUE* camera; "BP" refers to a bright pixel or cosmic-ray hit. A complete observing log is given in Table 2.

species: C IV, Si IV, C II, Si III, and Fe II. Haro 1 has a relatively flat spectrum; C IV, Si IV and the 1300 Å blend of Si II + Si III + O I are the most prominent features. The bump between 1460 and 1510 Å appears real and may partially be due to N IV] λ1486. This feature occurs frequently in long-exposure *IUE* spectra of blue galaxies (Rosa, Joubert, and Benvenuti 1984; Huchra *et al.* 1983), but its origin is uncertain. Haro 2 exhibits many well-defined lines, a rising continuum, and a C IV P Cygni profile. Haro 3 is similar in appearance to Haro 2 with weaker line features. The C IV emission spike is spurious, being due to a cosmic-ray hit or a bright pixel. Haro 15 is sufficiently distant for Lyα λ1215 to be redshifted away from the geocoronal Lyα emission present in all long *IUE* exposures. The overall spectrum is similar to that of Haro 3, and a moderate-strength intrinsic Lyα line is observed. An absorption feature at the laboratory wavelength of 1550 Å may be due to a Galactic component of C IV. Mrk 209 displays a more steeply rising continuum and weaker absorption lines than any other galaxy in this sample and is the only BCG to show a strong C III] λ1909 emission line. The weak absorption line strengths are probably related to the low metallicity of Mrk 209 ($Z_{gas}/Z_\odot \approx 0.1$) and the strength of the C III] emission to the high nebular temperature ($T_e \approx 14{,}500$ K; VT83). The spectra of Mrk 86 and VII Zw 403 are much noisier than the other five spectra, and no certain features can be identified. We note that spurious emission features are found in all spectra, especially a weak "line" seen near 1750 Å. This artifact is due to a few bright pixels offset from the central spectral order. It is observed in many long-exposure *IUE* spectra and has sometimes been misidentified as N III] λ1751.

The BCG spectra are *clearly composite* and display spectral features characteristic of a mixture of OBA stars as presented in the *IUE Spectral Atlas* and Paper I: C IV λ1550 and Si IV λλ1394, 1403, seen in O3–B1 stars; C II λ1335 and the blend of Si II, Si III, and O I at ~1305 Å arising in mid-B stars; and Al II λ1671 and the blend of Fe and Al lines at ~1855 Å found in A stars. Spectral indices, as defined in Paper I, for Si IV, C IV, the 1305 Å blend, and the 1620 Å blend of iron lines are given in Table 4. Equivalent widths are also given.

The C IV and Si IV resonance lines are important diagnostics for the stellar atmospheres of hot stars. All spectra with good signal-to-noise ratios (i.e., excluding VII Zw 403 and Mrk 86) display the blueshifted absorption wings indicative of mass loss in stellar winds from OB stars. Maximum wind velocities determined from the blue absorption edge are in the range of 2500–4000 km s^{-1}, with Haro 2 (3200 ± 300 km s^{-1}) having the most well-determined value. These rough values are probably overestimated, since wind velocities measured with low-resolution *IUE* spectra are often too large, especially when the features are blended (Böhm-Vitense, Hodge, and Boggs 1984). Terminal wind velocities of Galactic OB stars are correlated with spectral type, varying from 1600 km s^{-1} at O8 V to 3400 km s^{-1} at O3 with broad scatter (Garmany *et al.* 1981). Given the resolution of *IUE* and potential Galactic halo contamination, the BCG wind velocities agree with those determined for nearby stars.

If we consider the intrinsic monochromatic luminosity at 1510 Å uncorrected for intrinsic reddening within the *IUE* aperture, Haro 1 and Haro 15 are comparable to the most luminous BCGs in the ultraviolet; they radiate approximately

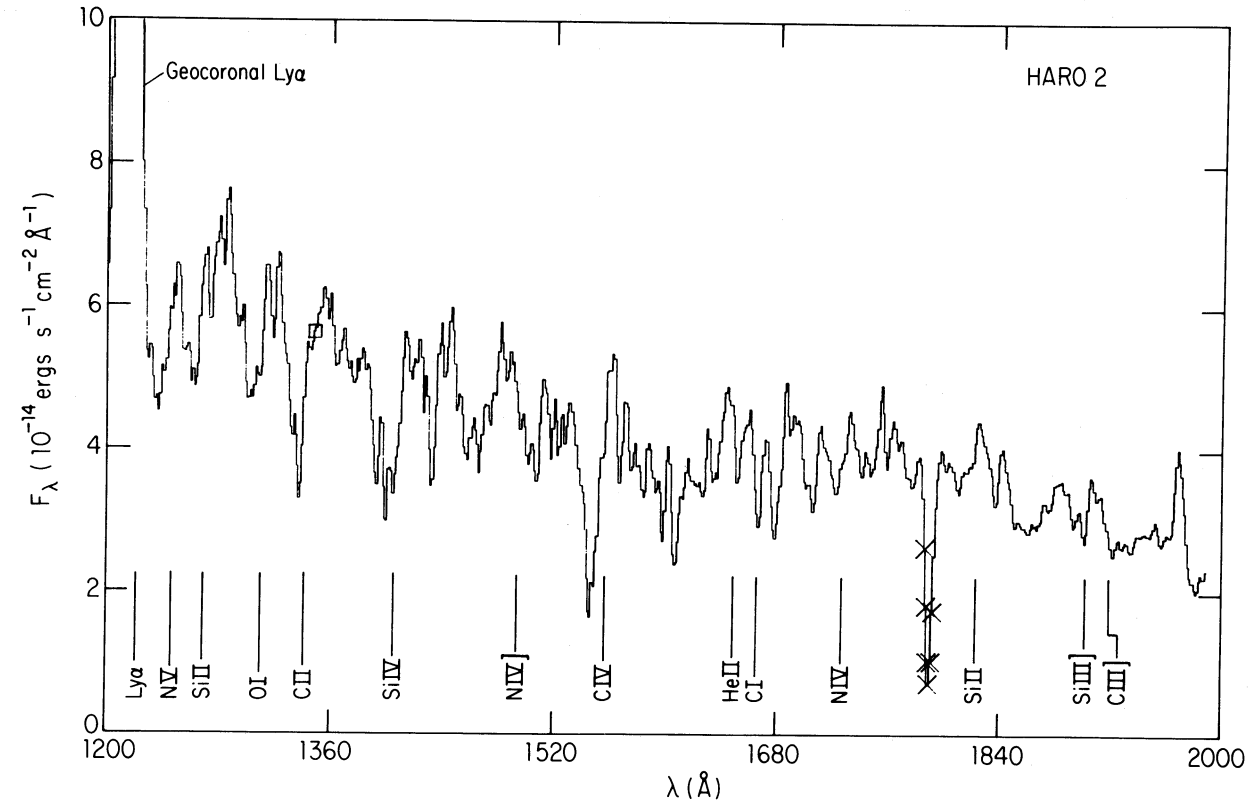

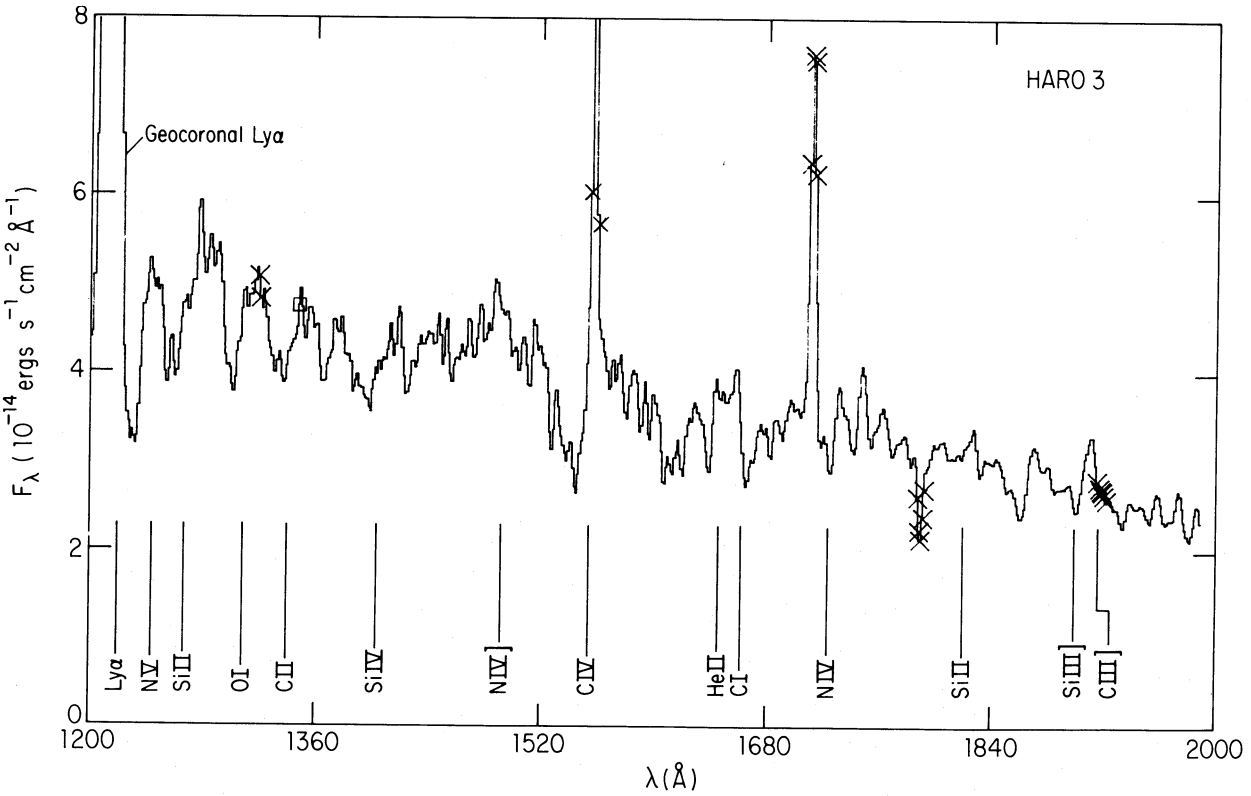

FIG. 1—*Continued*

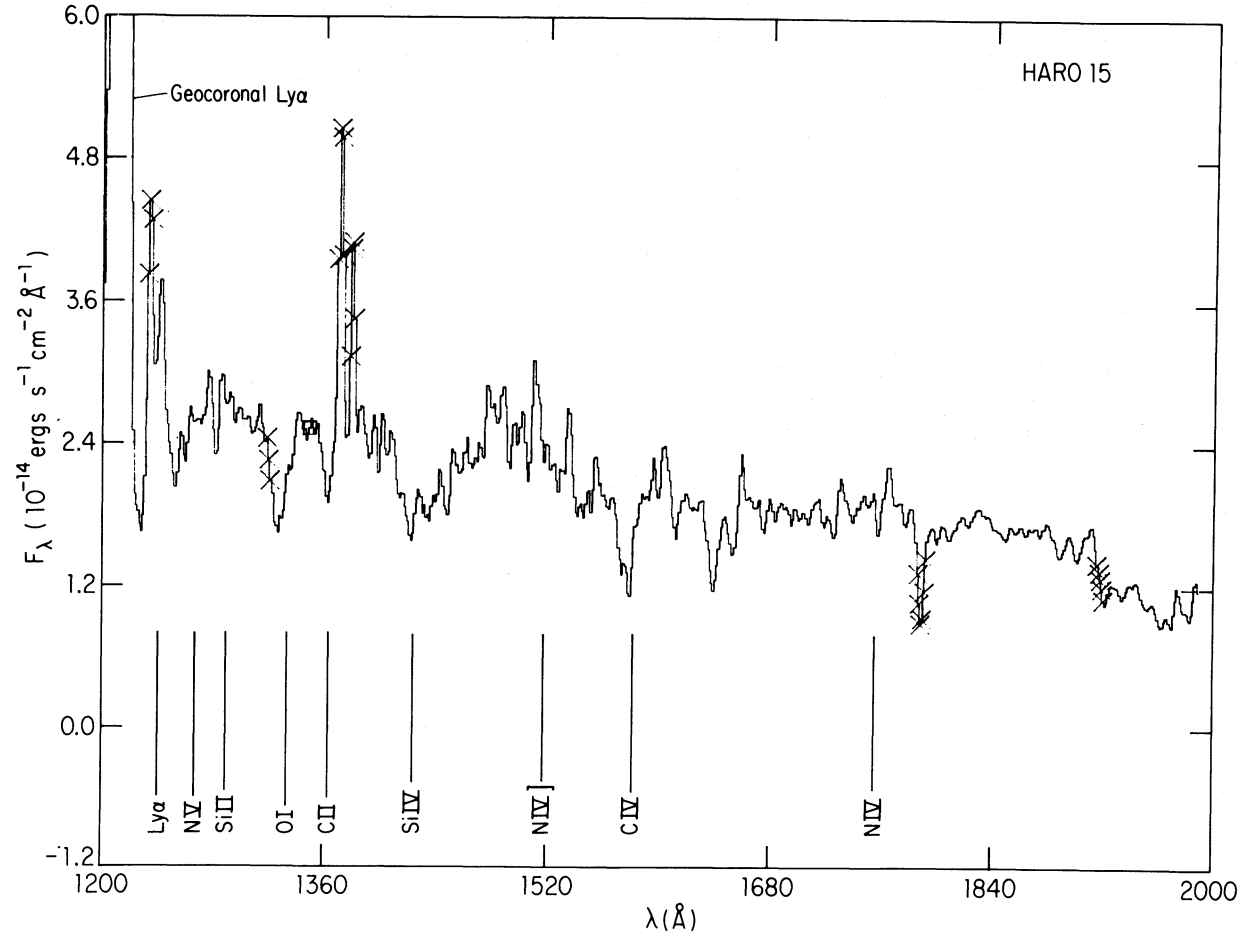

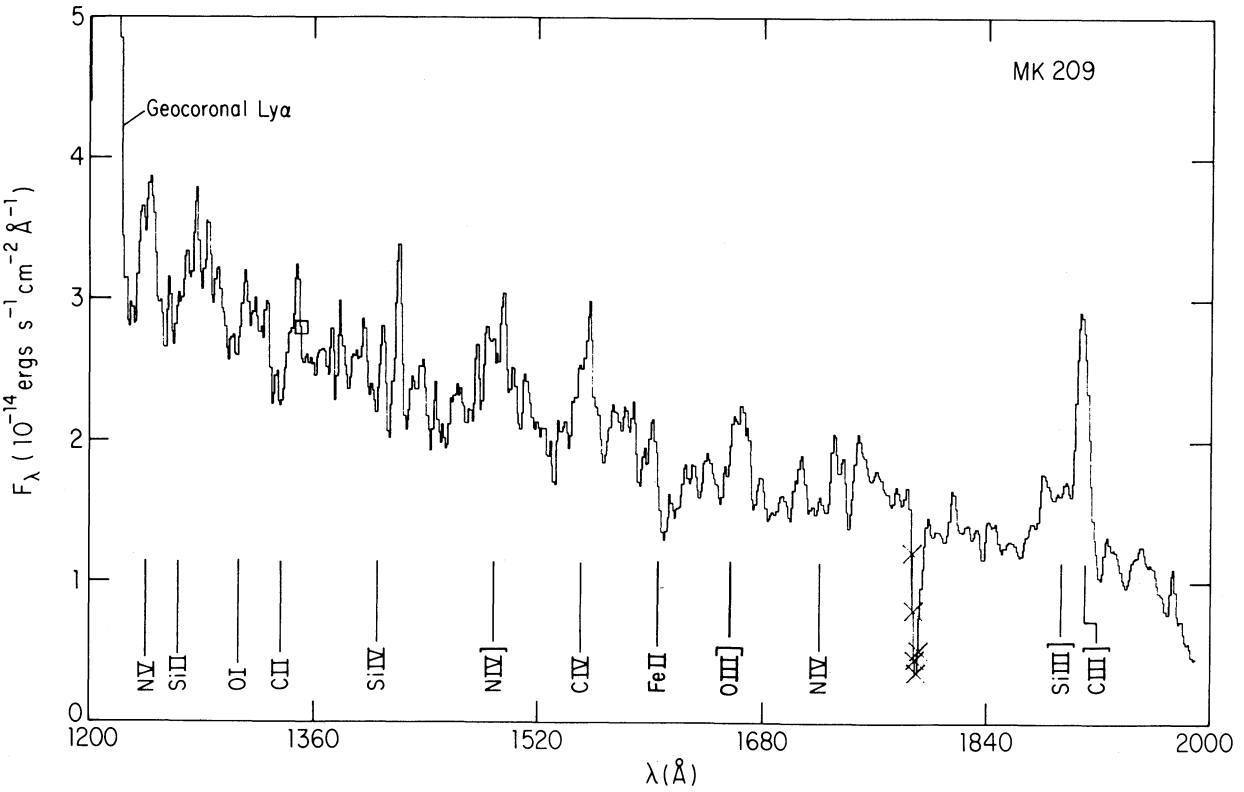

FIG. 1—*Continued*

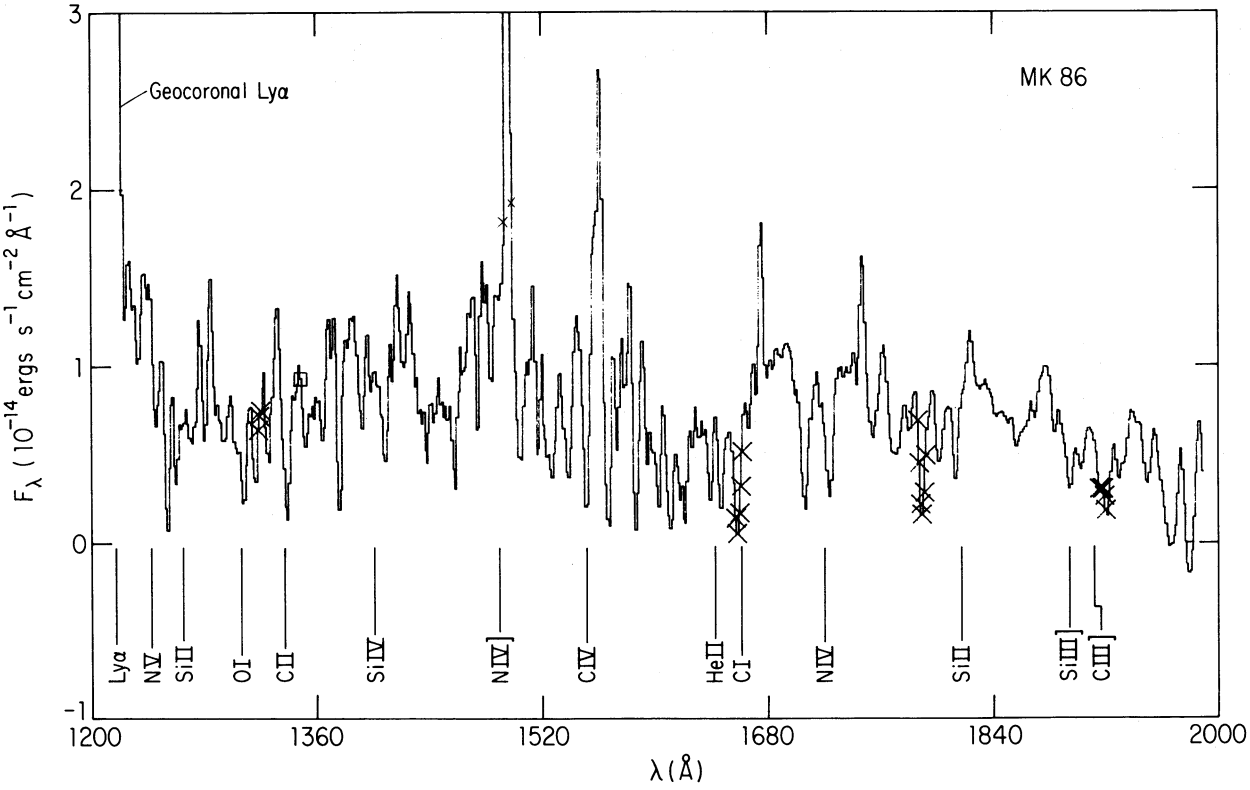

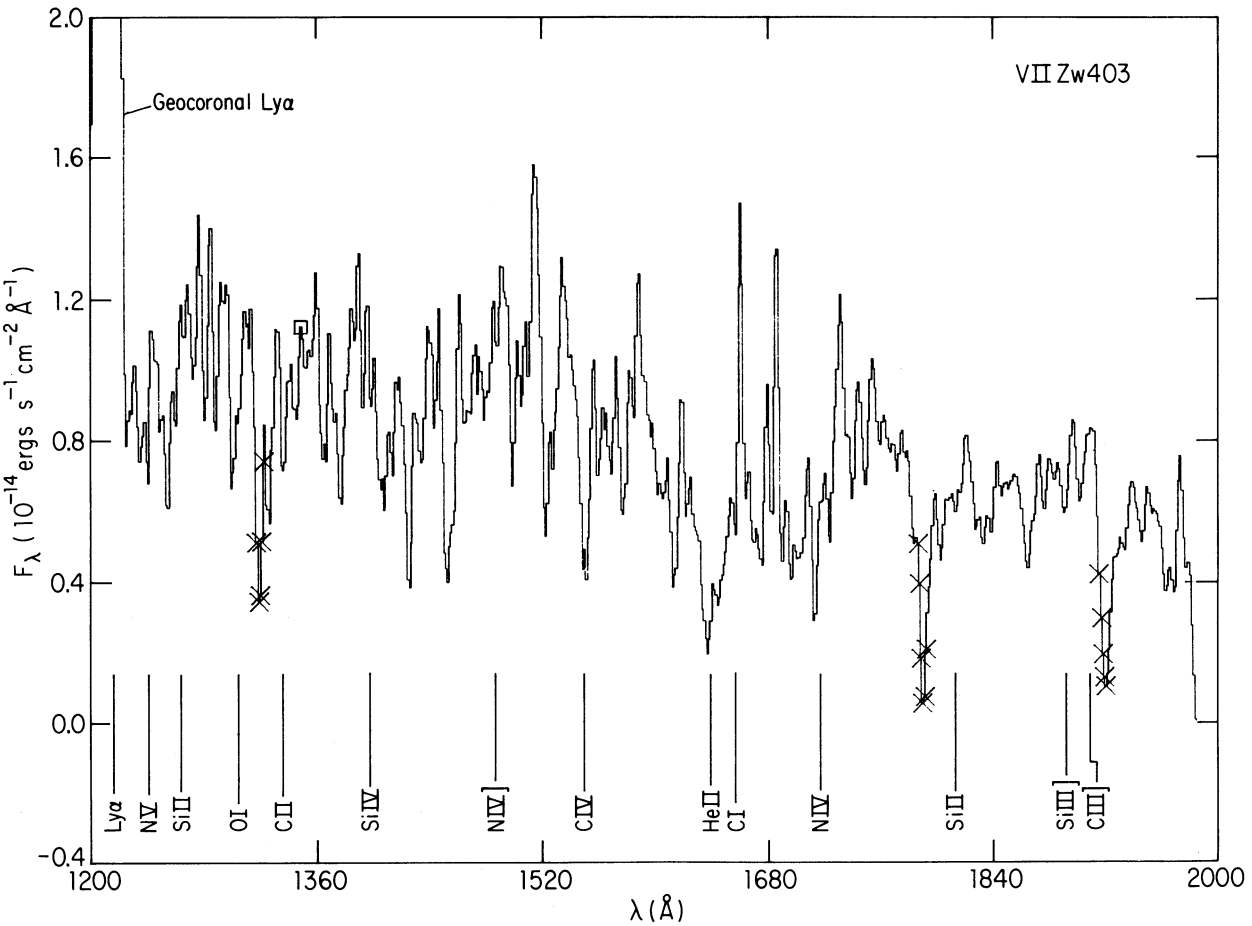

FIG. 1—*Continued*

TABLE 4

SPECTRAL INDICES AND EQUIVALENT WIDTHS[a]

Index	Haro 1	Haro 2	Haro 3	Haro 15	Mrk 209	VII Zw 403[b]	Mrk 86[b]
1305 Å	0.30[c]	0.16	0.17	0.23	0.12	0.03	0.43
	4.9	2.8	2.9	3.8	2.1	<1	6.5
Si IV λ1397	0.28	0.28	0.12	0.22	0.03	−0.15	0.03
	4.6	4.6	2.0	3.7	<1	<1	<1
C IV λ1540	0.44	0.28	0.23	0.34	0.13	0.09	0.01
	6.7	4.6	3.9	5.4	2.3	1.6	<1
C IV λ1550	0.30	−0.01[d]	...[e]	0.22	−0.05	0.35	−0.25
	4.9	<1	...	3.6	−1.0	5.5	−4.0
C IV λ1560	−0.01	−0.19[d]	...[e]	−0.05	−0.06	0.34	−0.35
	<1	−3.9	...	<1	−1.9	5.0	−5.5

[a] Spectral indices are defined as $I = -2.5 \times \log (F_\lambda / F^c_\lambda)$, where F_λ is the mean flux in a 20 Å bandwidth centered at λ, and F^c_λ is the continuum flux linearly interpolated from the bracketing sidebands (Paper I). These indices are expressed in magnitudes in the first row. The second row gives the corresponding pseudo–equivalent widths in angstroms with respect to the interpolated continuum, as defined by O'Connell 1973: $\mathrm{EW} = \Delta\lambda(1 - 10^{-0.4I})$.

[b] The spectra of VII Zw 403 and especially Mrk 86 have a low signal-to-noise ratio. Their spectral indices are poorly defined.

[c] This index is probably too large because of an anomalous emission feature in the blue sideband. An eye estimate gives EW ≈ 3 Å.

[d] The C IV indices for Haro 2 are underestimated because of bad data in the red sideband. For C IV λ1540, EW ≈ 6 Å.

[e] Cosmic-ray hit in the λ1560 bandpass. The C IV λλ1550, 1560 indices are spurious.

twice the flux of Mrk 325 at 1550 Å (Benvenuti, Casini, and Heidmann 1982*a*), or 10^3 times that of 30 Doradus in the LMC. Haro 2 and Haro 3 are an order of magnitude less luminous, and Mrk 209 is comparable to 30 Doradus. It is important to realize that the fixed *IUE* aperture contains quite different projected areas for each galaxy. For nearby galaxies such as Mrk 209, the UV light may arise from a single H II region, while for more distant galaxies such as Haro 15, several possibly noncoeval H II region complexes may contribute to the integrated luminosity. UV imagery with good spatial resolution, such as those to be returned by the ASTRO and HST missions, will be needed to determine the number and extent of these regions.

c) *Cross-Dispersion Profiles*

Cross sections of the *IUE* spectra perpendicular to the dispersion direction provide information on the spatial distribution of the star-forming regions. In Figure 2 we present cross-dispersion profiles (*dashed line*) calculated over the range 1300–1900 Å for Haro 1, 2, 3, 15, and Mrk 209. In each panel the *IUE* point-spread function (FWHM = 5.″25) taken from the *IUE Image Processing Manual* (Cassatella, Barbero, and Benvenuti 1983; Turnrose and Thompson 1984) is displayed as a solid line. It has been normalized by the peak intensity in each profile.

For Mrk 209 and Haro 2, the star-forming regions are unresolved. Haro 3 has one dominant component and an extended weak wing which is consistent with an Hα image published by Hunter (1982) and the broad-band imagery of Burenkov and Khachikyan (1986). With the quoted FWHM and the distances listed in Table 1, upper limits on the sizes of the star-forming regions are $\lesssim$500 pc for Haro 2, $\lesssim$350 pc for Haro 3, and $\lesssim$100 pc for Mrk 209. The more distant, luminous BCGs Haro 1 and Haro 15 exhibit more complicated profiles. The entire aperture is illuminated by the starburst region in which several star-forming complexes appear to be present. These two objects may be similar to the "clumpy irregulars" discussed by Benvenuti, Casini, and Heidmann (1982*a*, *b*). Alternatively, an apparent clumpy structure could result from variable extinction across the aperture. Loose and Thuan (1986) note that a *B*-band image of Haro 1 appears to show a dust lane. Regardless of the origin of structure in the UV brightness distribution, it is clear that *star formation in the more distant and luminous BCGs is distributed over a much larger region than in the nearby, lower luminosity objects.*

IV. SPECTRAL SYNTHESIS TECHNIQUE

a) *General*

Spectral synthesis is performed for a selected set of 18 bandpasses of 20 Å width in the range 1230–1900 Å, chosen according to methods developed in O'Connell (1973). A stellar library composed of 15 spectral groups was constructed from spectra published in the *IUE Spectral Atlas* (Wu *et al.* 1983). Complete details on the selection of the wavelength sequence, the library, and the basic stellar parameters adopted for the synthesis may be found in Paper I. For this study we have chosen to exclude stars of luminosity class III because of the similarity of both their broad-band ultraviolet-to-visible colors and their far-UV SEDs to main-sequence spectral types. We felt that the synthesis algorithm would not be able to distinguish adequately between main-sequence and giant stars in composite spectra. By including only main-sequence and supergiant types, we hope to measure the relative contributions of each more accurately.

The optimizing linear programming spectral synthesis technique described by O'Connell (1976) is applied to the far-UV data. For a given subset of the library of stellar SEDs, the algorithm finds the mixture which minimizes the mean absolute fractional residual between the galaxy SED and that of the mixture. The absolute value of the fractional residual is $r_i = |1 - y_i/z_i|$, where y_i is the total (normalized) flux of the model at wavelength i and z_i is the flux of the composite source. The quantity

$$q = \sum_{i=1}^{N-1} w_i r_i \,, \qquad (1)$$

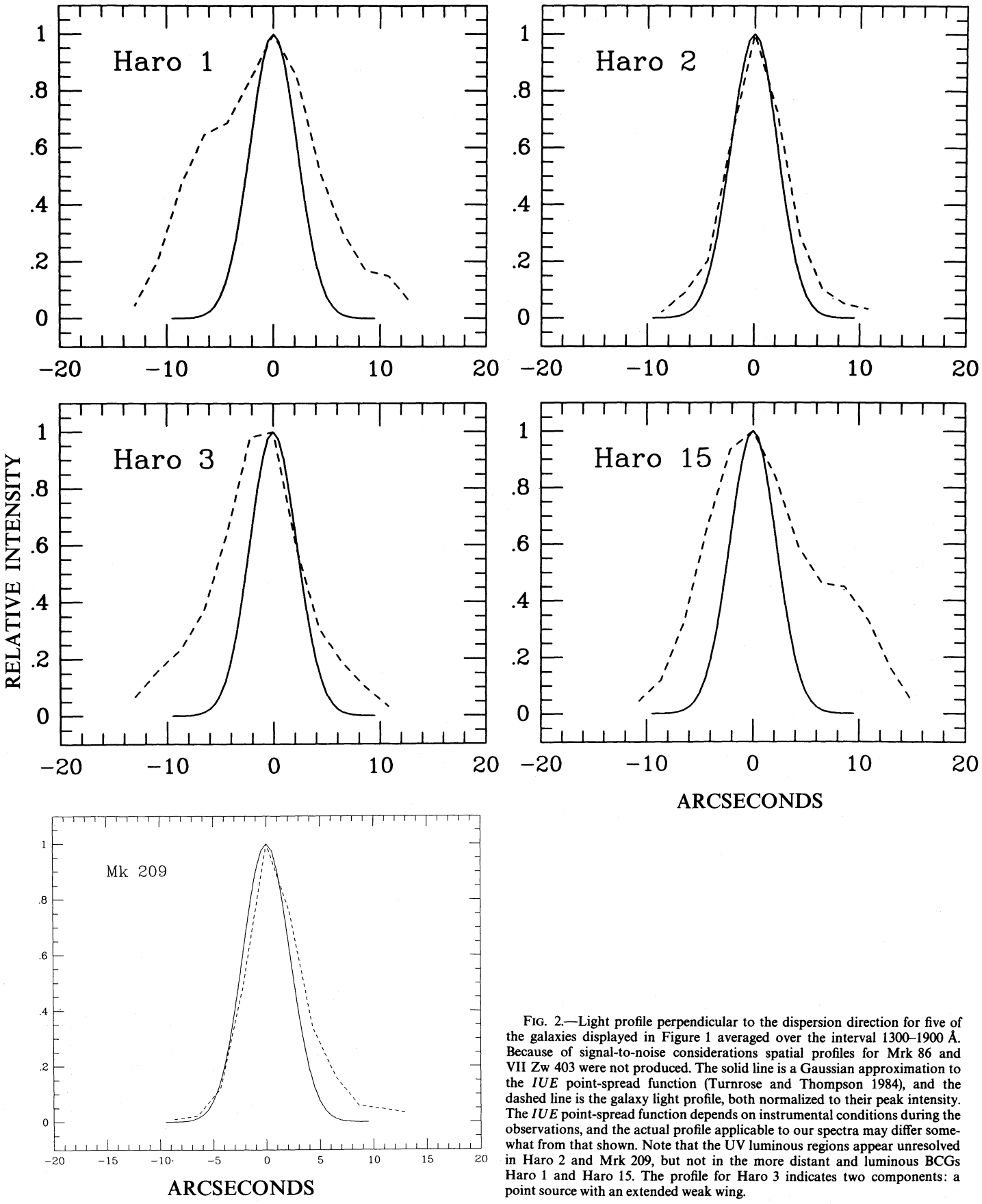

FIG. 2.—Light profile perpendicular to the dispersion direction for five of the galaxies displayed in Figure 1 averaged over the interval 1300–1900 Å. Because of signal-to-noise considerations spatial profiles for Mrk 86 and VII Zw 403 were not produced. The solid line is a Gaussian approximation to the *IUE* point-spread function (Turnrose and Thompson 1984), and the dashed line is the galaxy light profile, both normalized to their peak intensity. The *IUE* point-spread function depends on instrumental conditions during the observations, and the actual profile applicable to our spectra may differ somewhat from that shown. Note that the UV luminous regions appear unresolved in Haro 2 and Mrk 209, but not in the more distant and luminous BCGs Haro 1 and Haro 15. The profile for Haro 3 indicates two components: a point source with an extended weak wing.

where w_i is a weight given to the ith wavelength, is then minimized. We require $x_j \geq 0$, where x_j is the fraction of light produced by stellar type j at the normalizing wavelength. Solutions can be found for unconstrained mixtures of stellar types, or one can impose various sorts of linear equality constraints. The goodness of fit for each solution is expressed by ϵ, the mean absolute fractional residual averaged over all synthesis bandpasses and converted to a percentage:

$$\epsilon = \frac{100q}{\sum_{i=1}^{N-1} w_i} . \quad (2)$$

We note that this procedure fits line *and* continuum points simultaneously, using all the information present in the data. We expect reasonable synthesis solutions to give fits no poorer than about $1.5\epsilon_{obs}$ (O'Connell 1976) and to be free of systematic residuals.

b) *Normalizing Wavelength*

After some experimentation, we choose the normalizing wavelength, λ_N, to be the 1510 Å bandpass. The synthesis solution is forced to fit at λ_N, and a poor choice for this bandpass could affect the nature of the solution. For example, selecting a normalizing bandpass which includes one of the Balmer lines in an optical synthesis investigation would give gross mismatches if one used a stellar library containing only absorption features to fit a composite spectrum exhibiting emission. Ideally, the normalizing bandpass should be pure continuum, but no such "line-free" regions exist in nature. The normalizing wavelength of 1510 Å was selected here because it is in the middle of the available spectral range and is relatively line-free.

c) *Modeling Internal Extinction*

The intrinsic UV spectra of BCGs may be significantly altered by internal extinction. We therefore adopt a technique which solves *simultaneously* for the extinction and the stellar population. Similar approaches to determining extinction at optical wavelengths have been shown to give results which agree with independent estimates of reddening (e.g., O'Connell 1976, 1980; Turnrose 1976). Our method is as follows. For a given subset of the stellar library, and a given set of constraints on the components, we synthesize a sequence of extinction-corrected galaxy SEDs for a range of assumed $E(B-V)$ values. Negative values of $E(B-V)$ (corresponding to an observed SED which is bluer than the intrinsic SED) are included to model crudely situations where dust scattering dominates extinction. For each sequence, we examine the variation of ϵ with $E(B-V)$. For well-fitted SEDs, ϵ should exhibit a smooth decrease to a reasonably well-defined minimum. Poorer fits display broader minima (Fig. 3). In each case the adopted color excess is the median value within a range of $\sim 10\%$ of the absolute minimum and is indicated by a vertical bar in Figure 3. The method works because the overall slope of the SED is sensitive to reddening but the strengths of discrete features (lines, continuum breaks) are not. The color excess derived from synthesis techniques is an independent measure of the extinction and can be compared with that determined with other methods, such as the Balmer decrement or radio continuum observations. Note that we remove an estimated Galactic extinction component before synthesis is attempted but that the modeling is sensitive to all reddening. Therefore the derived "intrinsic" extinction may contain some residual Galactic component. Finally, we have assumed that all dust lies in a screen between us and the source. Mixed star/dust models could have been treated, but only at the cost of additional parameters, which are inappropriate for this first consideration of the problem.

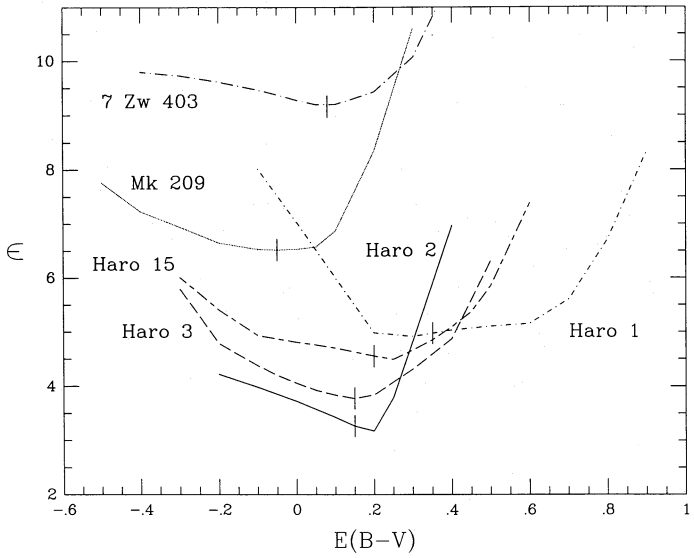

FIG. 3.—Dependence of the goodness-of-fit parameter ϵ for unconstrained optimized solutions on the amount of extinction assumed to affect the ultraviolet SED. The vertical bar on each curve indicates the adopted color excess (see § V*b*). Approximately 20 solutions are run for each object. Lower values of ϵ represent better fits to the data.

d) *Constraints*

Except for the exclusion of giant stars from the library, our initial solutions contain no constraints—i.e., no assumptions about the evolutionary history. Such unconstrained models provide the best obtainable fit with a given library and reddening law. We then explore the larger solution space by adding a variety of constraints, which are listed in Table 5. Constrained solutions are assessed by comparing their goodness-of-fit parameter ϵ and their distribution of residuals with wavelength with those of the unconstrained solutions.

Constraints of types A and B involve selectively deleting library components to test the ability of the modified library to fit the data. Solutions using constraint C test the significance of contributions from the coolest main-sequence group in our library, the A5–A7 V group, which displays a steeply rising continuum over the far-UV spectral range [Δm_λ(1355–1800) ≈

TABLE 5

TYPES OF CONSTRAINTS

Type	Definition
A	All luminosity class I groups excluded
B	All A star groups excluded (A0–A2 V, A5–A7 V, B8–A0 I)
C	A5–A7 V group constrained. ϕ(A5–A7) ≤ ϕ(A0–A2)
D	Nondecreasing main-sequence luminosity function
E1	Stellar group library replaced with a library of infinitely short burst models
E2	Stellar group library replaced with a library of continuous star formation models
F	Individual component maximum/minimum limit test

5 mag; see Fig. 5*b* of Paper I]. We also run a set of models (type D) with a requirement for a nondecreasing luminosity function, ϕ_j, on the main sequence, where groups are placed in order of increasing M_v. Here $\phi_j(M_v) = N_j/\Delta M_v$, and $\phi_{j+1}/\phi_j \geq 1.0$. N_j is the number of stars in group j, and ΔM_v is the range in absolute magnitude spanned by the group. We permit arbitrarily large jumps between successive groups.

We also synthesize the BCG spectra utilizing a library of synthetic SEDs (as opposed to the library of individual stellar groups described above), each representing an explicit star formation history (type E). These synthetic SEDs are further described in § VIII. This approach is equivalent to using the integrated SEDs of star clusters to model composite galaxy populations. Because the synthetic SEDs are forced to contain specified ratios of individual stellar groups, as in the "evolutionary synthesis" approach (Tinsley 1980), this procedure is a type of constraint.

Following O'Connell (1980), we can estimate the range of allowable amounts of a given stellar component by forcing successively larger (or smaller) contributions of that component and minimizing ϵ with respect to all other components until $\epsilon = \epsilon_{opt} + \Delta\epsilon$, where ϵ_{opt} is the optimal, unconstrained value and $\Delta\epsilon = 3\epsilon_{obs}/\sum w_i$. This is equivalent to a "3 σ" limit in the usual sense. This type of constraint (type F) is useful in comparing the synthesis-derived luminosity functions with possible analytic star formation histories and will be discussed in § VIII.

By the standards of most earlier synthesis investigations, the constraints imposed here are quite mild and permit identification of unusual population mixes or star formation histories which might be masked by stronger constraints. The constrained models employed are the simplest type which reflect the expected gross nature of the luminosity function.

e) Weights

Unit weight is assigned to all ultraviolet bandpasses except where examination of the photowrites showed data marred by bright pixels or cosmic-ray hits. Those points were given zero weight: λ1590 in Haro 2 and λ1560 in Haro 3; λ1550 was also given zero weight in any model where λ1540, λ1560 were given unit weight, since these bandpasses overlap. We also included *UBV* data derived from Huchra (1977*b*) and Longo and de Vaucouleurs (1983). These optical data were not included in the synthesis but serve as a consistency check.

f) Limitations

It is worth emphasizing that the utility of these models rests on several assumptions: that stars in the *IUE* atlas are representative of their spectral classification; that stars in the unknown composite SED are similar to library stars; that a standard reddening law (here Savage and Mathis 1979) applies; and that dust is present in a homogeneous screen in front of the luminous component. Incomplete stellar libraries are a difficulty for all integrated light studies (e.g., Burstein 1985), although optimizing synthesis techniques, by permitting internal adjustment of model parameters, are less sensitive to incompleteness than are evolutionary techniques. Our library lacks low-metallicity OB stars, for which there are no local analogs, yet some of our program galaxies (e.g., Mrk 209, which has $Z/Z_\odot \approx 0.1$) are known to be metal-poor. A symptom of the resulting library/galaxy mismatch will be absorption lines which are stronger in the model SED than in the galaxy SED.

As a test of the method, a set of composite UV SEDs was created from the library and synthesized as unknown spectra. The output mix of stellar components routinely reproduces the input mix. The results of these experiments show that components contributing less than $\sim$5% of the light in all synthesis bandpasses should be considered noise, while components with 5%–10% contributions are only marginal detections. While a putative component might be a major contributor at optical or infrared wavelengths, it cannot always be detected in the *IUE* spectra.

V. MODEL RESULTS

a) Unconstrained Solutions

Results of the unconstrained modeling of the far-UV spectra are presented in Table 6 and Figure 4. For each optimal solution, we give the fractional light contribution of each stellar component in three bandpasses, the population mix scaled to the reddening-corrected intrinsic luminosity, the difference in the strength of several spectral lines between the observed and the model SEDs, and a measure of the star formation and supernova rate derived from the massive star population. The latter quantities are discussed in § X. Figure 4 shows the difference spectra (observed minus model) for all of the bandpasses used in the synthesis. Note that the photometric errors are small ($\sim$0.02–0.04 mag) compared with the scale of the ordinate. The spectrum of Mrk 86 was too noisy to model and is not considered further. VII Zw 403 also displays poor signal-to-noise characteristics, but we did attempt crude modeling motivated by the availability of a detailed optical study (Tully *et al.* 1981) with which to compare the synthesis results.

We find generally good fits to the data: ϵ_{opt} ranges from 3.3 for Haro 2 to 6.5 for Mrk 209. For Haro 2 and Haro 3, $\epsilon_{opt} \approx \epsilon_{obs}$, while for Haro 1 and Haro 15, $\epsilon_{opt} \approx (1.35\text{–}1.45)\epsilon_{obs}$. Mrk 209 and VII Zw 403 give much poorer fits. The bad fit for VII Zw 403 is a consequence of the poor quality of the data. For Mrk 209, whose spectrum is well exposed, metallicity differences between the library and the galaxy appear to be the source of the larger discrepancy. We note that, given the small number of bandpasses (18), a large residual in a single bandpass can adversely affect ϵ_{opt}.

O stars are selected in all unconstrained solutions, as could be anticipated from the presence of C IV λ1550. Haro 2, Haro 3, and Haro 15 display similar stellar mixes: an O3–O6 V + early B component and a cooler A star population. Haro 1 has a dominant O9–B0 supergiant component, while Haro 15 includes a marginally significant mid-B supergiant population. Only the solution for Mrk 209 contains no starlight cooler than $\sim$B6. The strength of the A star component in the Haro galaxies is somewhat surprising and is discussed further in § V*d*.

The most striking result presented in Table 6 is that *no unconstrained solution shows a continuous main-sequence luminosity function.* The luminosity functions for all galaxies exhibit *both* missing groups *and* large jumps between selected groups. In particular, no main-sequence groups between spectral types $\sim$B2 and A0 are selected, except in Haro 3 (the B4–B7 V component found in Haro 15 contributes less than 5% of the light at all far-UV wavelengths and is considered noise according to the criteria described in § IV). It is important to note that the nonselection of a library member does not imply that such stars are absent from the galaxy. Rather, such groups contribute negligible light to the integrated UV SED.

TABLE 6

UNCONSTRAINED SOLUTIONS

	IIaro 1				IIaro 2				Haro 3				Haro 15				Mrk 209				VII Zw 403			
ϵ_{opt} [a]	4.97				3.26				3.77				4.55				6.52				9.16			
E(B–V) [b]	0.35				0.15				0.15				0.20				−0.05				0.08			
Group	N [c]	% light			N [c]	% light			N [c]	% light			N [c]	% light			N [c]	% light			N [c]	% light		
		λ1355	λ1510	λ1813		λ1355	λ1510	λ1813		λ1355	λ1510	λ1813		λ1355	λ1510	λ1813		λ1355	λ1510	λ1813		λ1355	λ1510	λ1813
O3–6 V	2.1+4	3.7	4.4	3.1	6.2+3	39.0	46.1	30.8	2.3+3	36.0	38.6	31.6	7.0+4	23.7	28.1	20.2	35	38.7	40.7	36.5	0.0	0.0	0.0	0.0
O7–B0 V	0.0	0.0	0.0	0.0	0.0	0.0	0.0	0.0	2.6+3	15.1	13.6	11.7	0.0	0.0	0.0	0.0	37	15.0	13.2	12.3	130	78.6	67.9	55.7
B1–1.5 V	2.6+6	28.9	24.2	22.9	1.4+5	58.3	48.0	37.0	0.0	0.0	0.0	0.0	2.7+6	58.5	48.4	39.9	0.0	0.0	0.0	0.0	0.0	0.0	0.0	0.0
B2–3 V	0.0	0.0	0.0	0.0	0.0	0.0	0.0	0.0	7.1+4	13.6	12.0	11.8	0.0	0.0	0.0	0.0	0.0	0.0	0.0	0.0	0.0	0.0	0.0	0.0
B4–7 V	0.0	0.0	0.0	0.0	0.0	0.0	0.0	0.0	1.0+6	35.3	35.7	36.4	3.9+6	2.9	3.3	2.9	1.9+4	46.3	46.1	51.2	0.0	0.0	0.0	0.0
B8–9 V	0.0	0.0	0.0	0.0	0.0	0.0	0.0	0.0	0.0	0.0	0.0	0.0	0.0	0.0	0.0	0.0	0.0	0.0	0.0	0.0	0.0	0.0	0.0	0.0
A0–2 V	1.2+9	3.1	7.0	12.2	2.7+7	2.6	5.6	9.5	0.0	0.0	0.0	0.0	5.2+8	2.6	5.9	10.7	0.0	0.0	0.0	0.0	0.0	0.0	0.0	0.0
A5–7 V	6.3+9	0.0	0.1	9.5	4.3+8	0.1	0.3	22.7	6.0+7	0.0	0.1	8.5	3.6+9	0.1	0.1	10.9	0.0	0.0	0.0	0.0	0.0	0.0	0.0	0.0
O9–B0 I	2.4+5	53.6	51.8	42.9	0.0	0.0	0.0	0.0	0.0	0.0	0.0	0.0	0.0	0.0	0.0	0.0	0.0	0.0	0.0	0.0	0.0	0.0	0.0	0.0
B3–5 I	2.9+5	10.7	12.5	13.2	0.0	0.0	0.0	0.0	0.0	0.0	0.0	0.0	1.7+5	12.2	14.2	15.5	0.0	0.0	0.0	0.0	0.0	0.0	0.0	0.0
B8–A0 I	0.0	0.0	0.0	0.0	0.0	0.0	0.0	0.0	0.0	0.0	0.0	0.0	0.0	0.0	0.0	0.0	0.0	0.0	0.0	0.0	42	21.4	32.1	44.3
Index	ΔI [d]				ΔI [d]				ΔI [d]				ΔI [d]				ΔI [d]				Δ I [d]			
1305 Å	0.18 [e]				0.06				−0.03				0.09				−0.05				0.00			
Si IV	0.04				0.07				0.01				0.04				−0.05				−0.20			
C IV λ1540	0.01				... [f]				−0.08				−0.01				−0.25				−0.23			
C IV λ1560	−0.02				... [f]				... [g]				−0.02				−0.01				0.13			
1620 Å	−0.01				... [f]				−0.01				−0.04				0.08				0.19			
$\dot{M}$ $(m/m_\odot \geq 10)$ [h]	3.30				0.15				0.03				2.80				4×10^{-4}				1×10^{-4}			
$\dot{M}$ $(m/m_\odot \geq 2)$ [i]	17				0.75				0.15				14				2×10^{-3}				1×10^{-3}			
SNR [j]	0.20				0.01				1.0×10^{-3}				0.20				1×10^{-5}				2×10^{-5}			

[a] The goodness-of-fit parameter (defined in the text) for the optimal, unconstrained synthesis solution. Smaller values of ϵ indicate better fits to the data.

[b] The reddening associated with the optimal solution. These values measure the extinction intrinsic to the object. The total extinction correction applied to each galaxy SED was the sum of the quoted values and the Galactic extinction given in Table 1.

[c] The total number of stars in each group derived from the unconstrained solution after scaling the extinction-corrected observed flux to the distances listed in Table 1.

[d] The difference in the strength of the given feature expressed in magnitudes in the sense of (galaxy minus model). A negative value indicates that the feature is stronger (weaker) in the model (galaxy).

[e] Possible contamination in the blue sideband gives an overestimate of the strength of this feature.

[f] Bad data in the red sideband produce spurious C IV indices for Haro 2.

[g] The λ1560 bandpass is affected by a bright pixel.

[h] The star formation rate in $M_\odot$ yr^{-1} for stars with $m/M_\odot \geq 10$. $\dot{M} = \sum (n_i m_i)/\tau_i$, where n_i is the number of stars in group i (given above) and τ_i and m_i are respectively the lifetime and mass of the group taken from Paper I. Note that this straightforward measure of the star formation rate makes no assumptions regarding the initial mass function.

[i] The star formation rate for stars with $m/M_\odot \geq 2$. $\dot{M} = A \int m\Psi(m)\,dm$. The normalization is determined by the formation rate of stars with $m/M_\odot \geq 10$. An IMF with $x = 1.8$ (see eq. [4]) is assumed, and the limits of integration, from 2 to 100, represent the mass range of stellar groups which produce appreciable flux in the far-UV.

[j] The number of supernovae expected per year determined as $\sum n_i/\tau_i$ for all groups with $m_i \geq 10$.

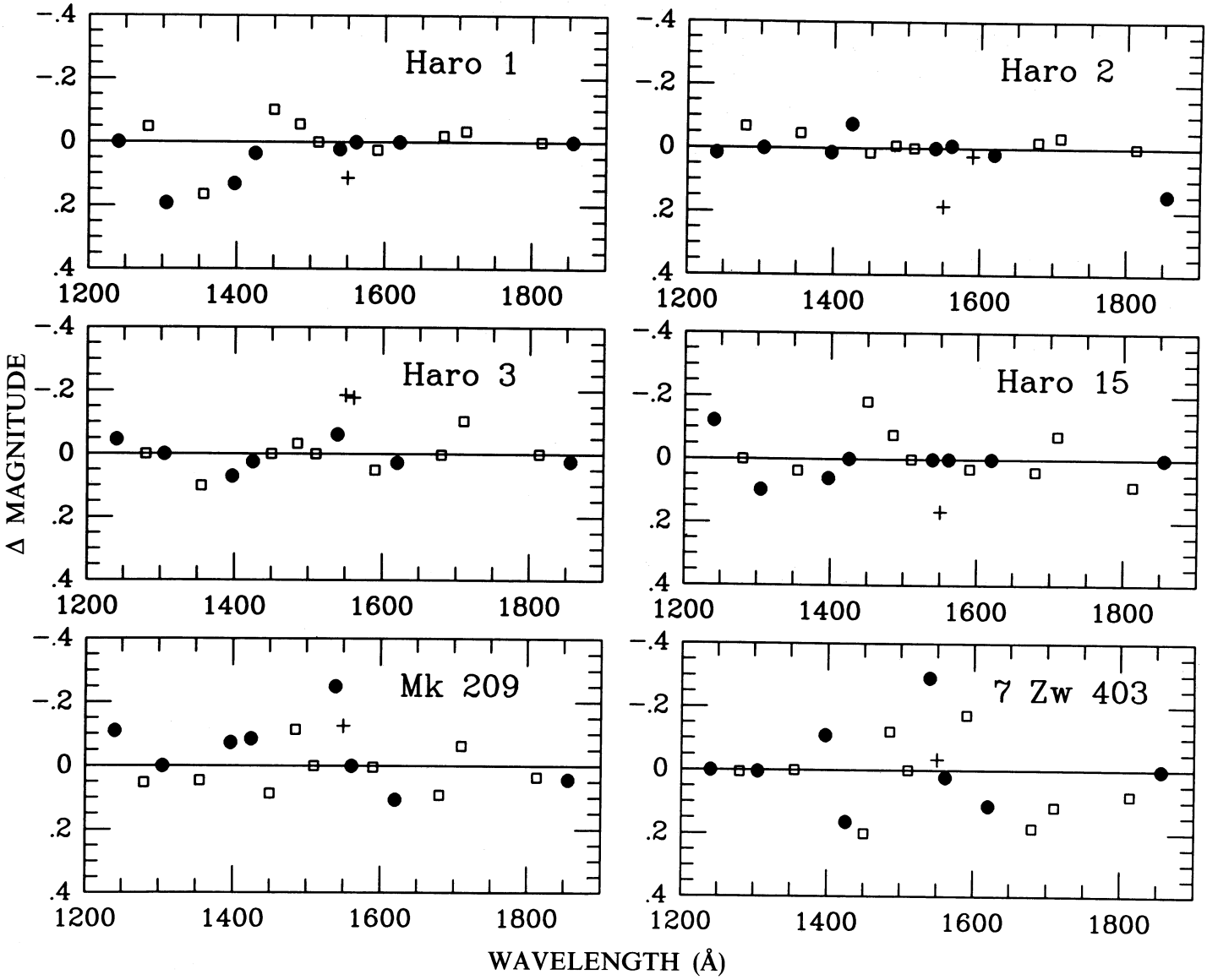

FIG. 4.—Flux residuals for the adopted optimal unconstrained solutions in the sense $\Delta M = M_{\text{galaxy}} - M_{\text{model}}$. The normalizing wavelength is 1510 Å. Details of the wavelength sequence are presented in Paper I. Filled circles represent bandpasses with prominent line features; open squares are primarily continuum bandpasses; and plus signs indicate bandpasses which were assigned zero weight in the synthesis.The λ1550 bandpass was given zero weight because of its overlap with the λλ1540, 1560 bandpasses.

Discontinuous luminosity functions suggest discrete episodes of star formation (bursts), where the end of a star formation episode corresponds to the main-sequence lifetime of the stars at a discontinuity. Continuous star formation would produce smooth luminosity functions. In § VIII we examine the implications of these results for the star formation history of BCGs.

b) Internal Extinction

The BCGs show a range of intrinsic extinctions. Optimal values of $E(B-V)$, given in Table 6, are correlated with the slope of the observed SED. Steep spectra (Mrk 209) have little to no extinction, while the flattest observed SED (Haro 1) exhibits the largest color excess. Note that, in contrast to the optical, there is in the UV a smaller likelihood of mistaking a cooler mix of stars for a larger reddening because of the fact that hot stars tend to have similar continuum slopes, while stars cooler than ~B5 have grossly different SEDs (cf. Paper I). All of the BCGs synthesized here exhibit a smooth decrease in ϵ with $E(B-V)$ and a more rapid increase after the minimum is reached, as illustrated in Figure 3. Similar behavior was found by Turnrose (1976) in an optimizing synthesis analysis of Sc spiral nuclei, and by O'Connell (1980) in estimating the foreground extinction for a sample of elliptical galaxies. Galaxies with larger values of ϵ display broader minima with corresponding larger uncertainties in the optimal value of $E(B-V)$. Estimated uncertainties in $E(B-V)$ are given in Table 6. Turnrose (1976) quotes errors of $\sim \pm 0.10$ for his sample. The optimizing synthesis approach appears to provide a quantitative measure of the amount of extinction affecting the optical/UV *continuum* energy distribution no less accurate than the Balmer decrement or radio continuum techniques.

TABLE 7

SUBOPTIMAL CONSTRAINED SOLUTIONS

Object	Constraint Type	ϵ/ϵ_{opt} [a]	Comments
Haro 1	A	1.38	68% of the light at λ1510 from O7–B0 V; ΔI(C IV λ1540) = 0.13, UNC = 0.01; ΔI(Si IV λ1397) = 0.12, UNC = 0.04
Haro 2	B	1.29	$\Delta m_{1710} \approx -0.1$ mag, UNC = −0.03
Haro 1	E1, 2	1.29	Supergiant groups produce 100% of the light
Haro 2	B	1.98	O3–O6 V ≈ 39%; B1–B1.5 V ≈ 42%; B3–B5 I ≈ 19%; all residuals λ > 1600 Å are negative; $\Delta m_{1710} \approx -0.2$ mag; UNC = −0.03
Haro 2	C	1.15	The mean residual for λ > 1650 Å (4 passes) = −0.1 mag
Haro 2	D	1.16	Groups not present in the unconstrained solution provide 24% of the light at λ1510
Haro 2	E1	2.93	25% x = 2.3 ISB model + 75% supergiants
Haro 2	E2	2.87	Systematic residuals; solution is O9–B0 I + 10^9 yr CSF model
Haro 3	B	1.15	15% of the light from B9–B9.5 V
Haro 3	D	1.02	Very similar to the unconstrained solution
Haro 3	E2	1.15	1.25 × 10^9 CSF model produces 97% of the light
Haro 15	A	1.02	B1–B1.5 V increased by 8%; B8–B9.5 V now contributes 7%
Haro 15	B	1.18	B3–B5 1 component increases from 14% to 42%
Haro 15	E1	1.69	25% x = 2.3 ISB model + 75% B3–B5 I
Haro 15	E2	1.61	52% 1.25 × 10^9 CSF + supergiants
Mrk 209	D	1.03	Groups forced into the solution provide 3% of the light at λ1510
Mrk 209	E1	1.13	93% x = 1.3 ISB model + 7% B8–A0 I

NOTE.—Percentages quoted here refer to the percent contribution of a given population at the normalizing wavelength. A negative residual implies that the galaxy is brighter than the solution at the specified wavelength. UNC ≡ unconstrained solution.

[a] ϵ/ϵ_{opt} is the ratio of the goodness of fit of the constrained solution to that of the optimal solution. Our "3 σ" criterion for acceptable models requires $\epsilon/\epsilon_{opt} \lesssim 1.15$.

c) Absorption Lines and the Low Metallicity of Mrk 209

Most line features are well matched by the models (see Table 6), including the putative interstellar lines of C II λ1335 and the blend at 1305 Å. The unconstrained solution for Mrk 209 clearly shows that the low gas metallicity found by VT83 is also a property of the stellar component. The weak C IV absorption line, and the nonexistent Si IV line, agree with the results of Hutchings (1982), who found weaker features in a sample of O stars in the LMC ($Z \sim 0.3\ Z_\odot$) and SMC ($Z \sim 0.14\ Z_\odot$). Garmany and Conti (1985) find also that terminal wind velocities are about 20% lower in the LMC when compared with Galactic stars of the same spectral type. The low metallicity of Mrk 209 ($Z \sim 0.1\ Z_\odot$, VT83) is responsible for the large mismatch between the model C IV strength and the observed value.

d) Constrained Solutions

Suboptimal constrained solutions test the significance of the optimal stellar mixture. Examples of some suboptimal solutions are given in Table 7 arranged by object. These solutions are characterized by ϵ/ϵ_{opt}, the ratio of the goodness of fit to its value for the corresponding unconstrained (optimal) solution.

The supergiant component found in Haro 1 appears real; a solution excluding supergiants produced a much poorer fit (model A). Haro 1 shows strong Si IV and 1620 Å features; both are indicators of supergiant light (Walborn and Panek 1984; Paper I). This was not true for Haro 15. In that case, excluding supergiants does not produce a significantly different ϵ. The B3–B5 I group in the unconstrained model for Haro 15 enters at the 10%–15% level and is only marginally significant.

Constraint type B explores the somewhat surprising A star component found in the Haro galaxies. We find that solutions which exclude the A groups result in much poorer fits, with systematic residuals at the wavelenths where those groups contribute significantly. Therefore, the UV data indicate that *a substantial A star component is present in the Haro galaxies and cannot be modeled with other groups.* In Haro 1, Haro 2, and Haro 15 the A groups contribute 20%–30% of the light in the λ1813 bandpass. In Haro 3 this component is present at just under 10% and would have to be considered a marginal detection.

We have checked the solutions by computing the *UBV* fluxes of the stellar mix in the unconstrained solutions and comparing these with observed values. The optical data consist of aperture photometry, which must be converted to an *IUE*–sized aperture using the magnitude-aperture curves of Huchra (1977*b*). Unfortunately, most of the available data were taken through apertures substantially larger than *IUE* and require an uncertain extrapolation. We find that optimal solutions containing an A star component predict more light in the *UBV* bandpasses than estimated, by 0.5–1.5 mag. This is troubling, since many cooler stellar types, which will contribute no light at far-UV wavelengths, should also be present in the optical window.

The excess light in the visual bandpasses produced by the unconstrained solutions is caused primarily by the presence of the A5–A7 V group. Constraint type C was imposed to examine the goodness of fit while reducing the visual flux of the solution. For Haro 2, ϵ is ∼30% larger and the "excess" V flux is reduced from ∼1.3 to 0.25 mag. Because it contributes at only the longest wavelengths within the available spectral range, the A5–A7 V group is at best weakly determined by far-UV synthesis. Essentially, the algorithm can adjust the coolest group to fit those few bandpasses with no effect on the bluer bandpasses. We believe the disagreement with the optical fluxes can be explained as a combination of (1) the uncertain extrapolation of the magnitude-aperture relation for the *UBV*

colors, (2) the uncertainty in the determination of the mid-A stellar population from far-UV spectra, and (3) extinction differences between the UV and visual regions (see § VI). We conclude that the A star component *is* real but that the luminosity function of the A5–A7 V group is poorly determined and may be overestimated. Extension of the analysis to the mid-UV range (Fanelli 1988) will provide a more accurate measure of the A star population.

Imposing a continuity constraint on the main-sequence luminosity function (type D) always produces solutions exhibiting a "flat" luminosity function ($\phi_{j+1} \approx \phi_j$) between the jumps observed in the optimal models. The parameter ϵ is larger but not greatly so, since components forced into the solution will not contribute much light. Attempts to force smooth luminosity functions—i.e., to require $\Delta \log \phi \approx$ constant between adjacent groups—produce substantially poorer fits, indicating that the jumps are real. This latter test is equivalent to modeling the SED with a continuous star formation scenario (constraint type E2).

VI. ULTRAVIOLET AND OPTICAL EXTINCTION

With the exception of Haro 1, total color excesses for the program galaxies are found to be small [$0.0 \leq E(B-V) \leq 0.20$]. Relatively low extinction in some star-forming galaxies has been noted previously (Huchra *et al.* 1983; Lamb *et al.* 1985). Despite the rise in the extinction function in the far-UV, these actively star-forming regions are evidently *not heavily obscured* even though substantial amounts of neutral gas (Thuan and Martin 1981; Gordon and Gottesman 1981) and dust are present (Kunth and Sevre 1986; Thronson and Telesco 1986). A definite trend is present in the UV extinction measures: the nearby, low-luminosity dwarfs have negligible extinction (which may arise completely in the Galaxy), the two intermediate-luminosity objects have $0.10 \leq E(B-V) \leq 0.15$, while the two luminous galaxies have somewhat larger values. For nearby objects the *IUE* aperture sees only a single dominant star formation region, which can be characterized by a single color excess. In Haro 1 and Haro 15, where a much larger area is observed (containing several star-forming complexes as shown by the cross-dispersion profiles [Fig. 2]), variable extinction across the region observed by *IUE* is the most likely explanation for the larger total extinction and the broader ϵ–$E(B-V)$ relation (Fig. 3). As mentioned in § III, the surface photometry of Loose and Thuan (1986) indicates that a dust lane is present in Haro 1.

Synthesis-derived extinction measures can be compared with those derived from the Balmer decrement or thermal radio continuum fluxes. With the caveat that different apertures were used at different wavelengths (a problem of some importance in multifrequency spectral modeling of complex stellar populations), we compare our values of $E(B-V)$ with values taken from the literature. These data are given in Table 8. Four of the six galaxies have extinction measures derived from Balmer lines. In each case, the UV synthesis–derived color excess is smaller than that determined from the Balmer decrement. For Mrk 209 and VII Zw 403 we find that $E(B-V)_{\rm Balmer} - E(B-V)_{\rm UV} \approx 0.3$. Clearly, the extinction implied by the optical spectrophotometry is not applicable to the ultraviolet unless the reddening law is much *less* steep than the Galactic law.

If the UV spectrum of Mrk 209 were dereddened by the amount implied from the Balmer lines, the intrinsic far-UV continuum would be bluer than the hottest stellar groups [$\Delta m_\lambda(1355\text{–}1710) \approx -0.97$, compared to -0.73 for the O3–O6 V group]. A similar situation exists for VII Zw 403, where Tully *et al.* (1981) find $0.5 \leq E(B-V) \leq 0.7$, much larger than the $E(B-V) \approx 0.08$ derived from the synthesis method. But if the luminous component is stellar, the dereddened SED *cannot be steeper than the hottest stars.* For galaxies whose observed SEDs approach those of the first few library groups, little additional extinction is therefore allowed. In the low metallicity BCGs the continuum extinction may be slightly underestimated [$\Delta E(B-V) < +0.10$] if the intrinsic continua of metal-poor O stars are steeper over this wavelength range because of reduced metallic line blanketing (Massa and Savage 1985). The problem cannot be solved by adopting the reddening laws proposed for the LMC (Nandy *et al.* 1980) and the SMC (Rocca-Volmerange *et al.* 1981). That approach would in fact only exacerbate the discrepancy, since those reddening laws are steeper at shorter wavelengths than the Galactic law (Savage and Mathis 1979).

These results imply that the overall SED is subject to variable extinction—in particular, the UV-luminous population is seen through windows of low optical depth. (The same effect is often encountered when comparing thermal radio continuum data to the Balmer decrement: less extinction is implied by the optical data than by the radio data.) The lack of heavy extinction (again excluding Haro 1) implies a low dust content in the UV-emitting regions, especially in the low-luminosity dwarfs, which were not detected by *IRAS*. There appears to be a positive correlation between dust content and metallicity. The most metal-deficient BCGs, Mrk 209 and VII Zw 403, are found to have the lowest UV extinction, with correspondingly larger values for the more luminous objects. Also, the visibility of O stars with lifetimes less than ~ 5 Myr implies that the dust is efficiently destroyed or removed from the vicinity of the O stars by the combined action of ionizing radiation, stellar winds, and supernovae.

VII. A STELLAR ORIGIN FOR LOW-IONIZATION ABSORPTION LINES

Interpretation of the absorption lines present in the far-UV spectra of star-forming galaxies has had a checkered history. Many authors attribute an interstellar origin to the low-ionization lines (C II, Si II, Al II, S II, Fe II). These are assumed to be produced by a combination of intrinsic and Galactic absorption. Only high-ionization lines (Si IV, C IV, N IV, N V) are thought to arise in stellar atmospheres, and the low-ionization lines are frequently ignored in discussing the stellar content. However, all ionization states can have *both* an interstellar *and* stellar origin (see Lamb *et al.* 1985 for a similar discussion). Inspection of the *IUE Spectral Atlas* and the stellar library presented in Paper I shows that many of the lines routinely described as interstellar are prominent features in the far-UV spectra of B and A stars. Our optimizing synthesis approach has shown that most spectral features—*including* the so-called interstellar lines—are well matched by the solutions and arise naturally in the stellar component of star-forming regions.

Thus there is little evidence for an interstellar origin for most low-ionization species. The spectra of Haro 1 and Haro 15, whose redshifts are large enough to separate intrinsic from local components, show no features at the rest wavelengths of those species, indicating a negligible Galactic absorption-line component. However, the Galactic halo may contribute to the C IV line. Weak features are observed at 1550 Å in Haro 1 and Haro 15 distinct from the intrinsic redshifted C IV. For gal-

TABLE 8

COMPARISON OF UV-DETERMINED PARAMETERS TO VISUAL/RADIO DETERMINATIONS

Haro 1		Haro 2		Haro 3		Haro 15		Mrk 209		VII Zw 403	
UV	Visual/ Radio	UV	Visual/ Radio	UV	Visual/ Radio	UV	Visual/ Radio	UV	Visual/ Radio	UV	Visual/ Radio
Color Excess $E(B-V)$ (mag)[a]											
0.35	...	0.15	0.33[b] 0.32[c]	0.15	0.42[c]	0.20	...	−0.06 0.18[d]	0.30[d]	0.08	0.5–0.7[e]
6 cm Flux (mJy)[f]											
12	33[g]	8	12[g]	6	15[g]	5	13[g]	0.9	1.25[h]	0.1	...
Hα Flux (ergs s^{-1} cm^{-2})[i]											
3.9E−12	...	5.2E−12	...	4.3E−12	2.0E−12[j]	2.7E−12	...	9.1E−13	6.3E−13[d]	7.2E−14	9.7E−14[e]
Ionizing Photon Rate (s^{-1})[i]											
2.6E+54	...	2.9E+53	...	1.1E+53	3.0E+52[j]	3.3E+54	...	1.6E+51	1.9E+51[d]	9.3E+49	5.0E+50[e]

NOTE.—UV: values derived from optimizing synthesis of the ultraviolet SEDs reported here. Visual/radio: values obtained from optical or radio observations compiled from the literature or our own data.

[a] A measure of the reddening affecting the ultraviolet SED (observed through the 10″ × 20″ *IUE* aperture) is provided by the synthesis as described in § V*b*. These values are systematically lower than those determined from optical Balmer line ratios.

[b] Derived from the observed Hα/Hβ line ratio observed through a 2.″5 aperture by Hunter, Gallagher, and Rautenkranz 1982.

[c] Derived from IIDS spectra taken by Thuan 1981 with a 6″ aperture. After a correction for underlying stellar absorption, the Hβ/Hγ/Hδ line ratios were fitted to a case B recombination spectrum.

[d] These data are from Viallefond and Thuan 1983. An optical color excess of 0.30 is derived from Balmer line ratios based on IIDS spectra taken with a 6″ aperture. No correction for stellar absorption was necessary. An ionizing photon rate is determined from the 6 cm radio continuum flux. The extinction affecting the UV emission line C III] λ1909 was estimated from a comparison of the observed line flux to a theoretical C III]/Hβ ratio taken from the H II region models of Stasinska 1982. This extinction (A_{1909} = 1.44 mag) corresponds to $E(B-V)$ = 0.18 for the adopted (Savage and Mathis 1979) reddening law. The trend is $E(B-V)$ (UV continuum) < $E(B-V)$ (UV line emission) < $E(B-V)$ (optical line emission).

[e] Tully *et al.* 1981 have taken calibrated image-tube spectra corresponding to an aperture of 6″. The color excess was estimated from the Balmer line ratios. Note that their ionizing photon rate is derived assuming a reddening correction of $E(B-V) \sim 0.7$, whereas we have applied an $E(B-V)$ = 0.16 (0.08 internal, 0.08 Galactic).

[f] Radio fluxes derived from the synthesis are estimates of the thermal continuum flux produced by the ionizing population within the 10″ × 20″ aperture of the *IUE* spectrograph.

[g] These data are total flux measurements made with a beam size of 2.′46 taken from the survey of Klein, Wielebinski, and Thuan 1984.

[h] Viallefond and Thuan 1983 present a radio map taken with the Westerbork Synthesis Radio Radio Telescope. The indicated flux is the total flux from a thermal source whose spatial extent is smaller than the area observed with *IUE*. The predicted and observed values agree to within ∼30%.

[i] The Hα flux and ionizing photon rate are determined from the stellar population derived by the UV synthesis as described in § X. They are applicable to the spatial area observed by *IUE*. An extinction correction has been applied to produce the listed Hα flux; $E(B-V)_{\rm total} = E(B-V)_{\rm UV} + E(B-V)_{\rm G}$.

[j] The flux within a 9″ aperture determined from a KPNO video camera Hα image presented by Hunter 1982. No correction for underlying stellar absorption, contamination by [N II] lines, or extinction was applied. The ionizing photon rate is derived from the observed Hα flux and the assumed distance of 13.9 Mpc.

axies with recession velocities less than about 2000 km s^{-1} any Galactic halo component will be blended with the blueshifted wing of the intrinsic C IV profile. We note one feature, Fe II λ1608, which is observed in most objects but is poorly fitted by the models. This line may have an interstellar origin intrinsic to the BCGs.

VIII. STAR FORMATION HISTORY

The optimizing synthesis solutions discussed in § V exhibit discontinuous luminosity functions, which suggest a series of discrete star formation episodes or bursts. Here we evaluate these luminosity functions in terms of simple evolutionary models for the star formation history. The parameters which define an evolutionary model are $\Psi(m)$, the initial mass function (IMF), and $b(t)$, the temporal evolution of the total star formation rate (Tinsley 1980). The two limiting forms we will consider are the infinitely short burst (ISB), where $b(t)$ is a delta function at $t = 0$ (Lequeux *et al.* 1981; VT83), and continuous star formation (CSF), where $b(t) = b_0$, a constant, for $0 \lesssim t \lesssim t_{\rm CSF}$. We constructed a set of model luminosity functions for both ISB and CSF models according to equation (3), which gives the number of stars formed in the mass range m to $m + dm$ in the interval t to $t + dt$:

$$\zeta(m, t)dm\,dt = \Psi(m)dm\,b(t)dt\ . \tag{3}$$

Our models adopt the usual power-law approximation for the IMF,

$$\Psi(m)dm = Am^{-(1+x)}\,dm\ , \tag{4}$$

where $\Psi(m)$ is the number of stars formed in the mass range m to $m + dm$ and A is an arbitrary normalization constant. The total mass formed is thus

$$M_{\rm tot} = A\int_{m_l}^{m_u} m\Psi(m)\,dm\int_0^t b(t)\,dt\ , \tag{5}$$

where m_l and m_u are the lower and upper mass limits for the range of stellar types under consideration.

For the ISB models, the number of stars in population group i is

$$n_i = A\int_{m_{l,i}}^{m_{u,i}} m^{-(1+x)}\,dm\ , \tag{6}$$

TABLE 9

MODEL LUMINOSITY FUNCTIONS

Model	x[a]	t[b]
Infinitely Short Burst		
I1	1.3	<5
I2 ≡ C1	1.8	<5
I3	2.3	<5
Continuous Star Formation		
C2	1.8	10
C3	1.8	100
C4	1.8	1250

[a] Power-law slope of the initial mass function, defined by $dN/dm \propto m^{-(1+x)}$; $x = 1.35$ is the Salpeter value.

[b] Time scale in Myr for continuous star formation.

where the limits of integration represent the mass range of each stellar group. For CSF models proper account of evolutionary time scales must be made. Here

$$n_i = Ab_0 t_{\rm CSF} \int_{m_{l,i}}^{m_{u,i}} m^{-(1+x)}\, dm \quad \text{for } \tau_i > t_{\rm CSF}\,, \tag{7a}$$

$$n_i = Ab_0 \tau_i \int_{m_{l,i}}^{m_{u,i}} m^{-(1+x)}\, dm \quad \text{for } \tau_i \le t_{\rm CSF}\,, \tag{7b}$$

where τ_i is the stellar group lifetime adopted in Paper I. The resulting luminosity function is then $\phi_i = n_i/(\Delta M_v)$, where the absolute V-magnitude range of the group is taken from Paper I. We consider three ISB models, each with different IMF slopes, and three models with different $t_{\rm CSF}$ but with the same IMF slope, $x = 1.8$. This is the slope of the solar neighborhood mass function in the stellar mass range of interest (Scalo 1986). The parameters of these models are listed in Table 9.

We use the resulting model luminosity functions to test the unconstrained solutions in two complementary ways. First, we have computed synthetic SEDs for each luminosity function, substituted these for the individual stellar group SEDs in the library, and obtained new optimized solutions. These are called type E solutions in Table 7. Only ISB models were included in type E1 solutions and only CSF models models in type E2. Supergiant groups were included in both libraries as separate entries without constraints, since we did not feel that we could adequately predict their contributions given the uncertainty in post–main-sequence evolution of massive stars (§ II).

Type E1 ISB models cannot adequately fit the data (see Table 7). In most cases, the solutions contain the $x = 2.3$ ISB model and supergiant light but cannot produce a fit within the adopted limits. In Mrk 209, for which $\epsilon_{3\,\sigma} = 7.14$, a solution containing 90% ISB ($x = 1.3$) + 10% B8–A0 I is obtained with $\epsilon = 7.33$. Considering the lack of SEDs with appropriate metallicity in our library, this ISB model provides an acceptable fit.

We see from Table 7 that the type E2 CSF models *also* do not fit the data within the 3 σ limit for any object except Haro 3, where the $t_{\rm CSF} = 1.25$ Gyr model gives $\epsilon = 4.32$, and $\epsilon_{3\,\sigma} = 4.35$. Therefore, long-term star formation at the current rate implied by the most massive stars is ruled out. Similar evidence for episodic star formation was found by O'Connell (1983) for the nucleus of M33.

In the second approach, we compare the simple model luminosity functions *directly* with the luminosity functions derived from the unconstrained solutions. The component limit test (constraint type F) is used to estimate 3 σ upper and lower bounds on the contribution of each main-sequence group. Each panel of Figure 5 shows the luminosity function derived from the unconstrained solutions, with upper and lower limits, compared with the ISB and CSF model luminosity functions. The main-sequence lifetime of each group is also indicated.

There are several points to keep in mind while interpreting these figures. The technique used to derive the plotted limits on any component was to fix its value of ϕ_i and allow *all other* components to vary without constraints (except nonnegativity) to produce a new optimal solution. This process was repeated in order to locate the ϕ_i for which $\epsilon(\phi_i) = \epsilon_{\rm opt} + (3\epsilon_{\rm obs}/\sum w_i)$ (see § IV*d*). The resulting limits are therefore conservative, and the error bars are significantly larger than if they had been estimated from $\partial\epsilon/\partial\phi_i$. We have normalized the luminosity functions in Figure 5 to the O3–O6 V group. The uncertainty in ϕ for this group must be kept in mind as well. Moreover, the plotted limits themselves are *interdependent* and should not be viewed as unrelated observational errors. When one stellar group is constrained, the optimizing algorithm tends to adjust adjacent groups to compensate. Thus, if the O3–O6 V group is forced to a minimum, the O7–B0 V group is often adjusted to a maximum. In general, components of similar temperature therefore cannot be near their 3 σ limits simultaneously (except in the case of lower limits for components absent from the unconstrained solution). For example, in Haro 1 and Haro 15 either the A0–A2 V or the A5–A7 V group can be deleted, but not both. To put all this another way, an *arbitrary* curve drawn within the limits shown in Figure 5 will not necessarily yield an ϵ within the 3 σ limit.

We see from Figure 5 that the upper limit on the O7–B0 V component provides a stringent constraint on the duration of the *current* burst of star formation in Haro 2, Haro 15, and Mrk 209, which must be <10 Myr unless the IMF has $x \le 0$. The luminosity function for the B and A stars ($M_v > -3$) in Haro 2 indicates at least two bursts of star formation, the most recent of which ended not more than ~20 Myr ago. These were of larger amplitude than the current burst (the expected $\Delta \log \phi$'s for a discrete set of equal-amplitude bursts would be only 0.3). In the case of Haro 3 and Haro 15, the limits on star formation prior to 20 Myr ago are consistent with either a few isolated bursts or continuous star formation through the last Gyr. Note that a series of bursts of short duration (say ~5 Myr bursts separated by ~20–30 Myr) would mimic continuous star formation at the temporal resolution attainable in Figure 5 for $M_v \ge -3$. In Haro 1 the data permit the hottest main-sequence group (O3–O6 V) to be deleted altogether, and there is good evidence for a strong supergiant component (cf. § IX), suggesting that star formation ended ~3–5 Myr ago there. Limits on the earlier history of star formation are similar to those for Haro 3 and Haro 15. In none of these cases except Haro 2 do the formal error bars of Figure 5 exclude the ISB luminosity functions; however, as noted above, when these are actually placed in the synthesis library, the resulting fits are not within the 3 σ limits.

In Mrk 209 the jump in the luminosity function at $M_v = -1$ may indicate the main-sequence turnoff of a burst which occurred ~50–100 Myr ago. But it is also possible, given the low metallicity of this BCG, that this represents a population

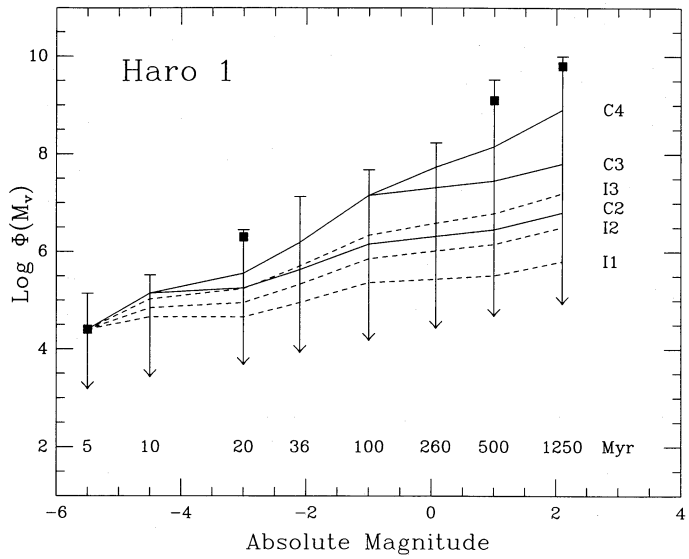

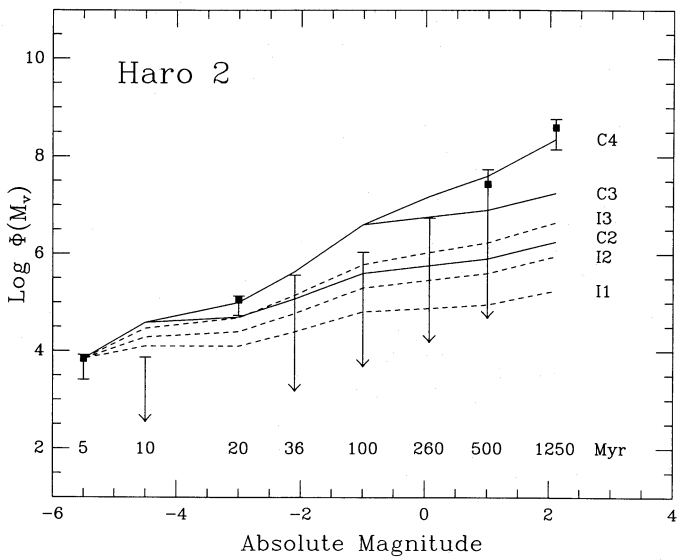

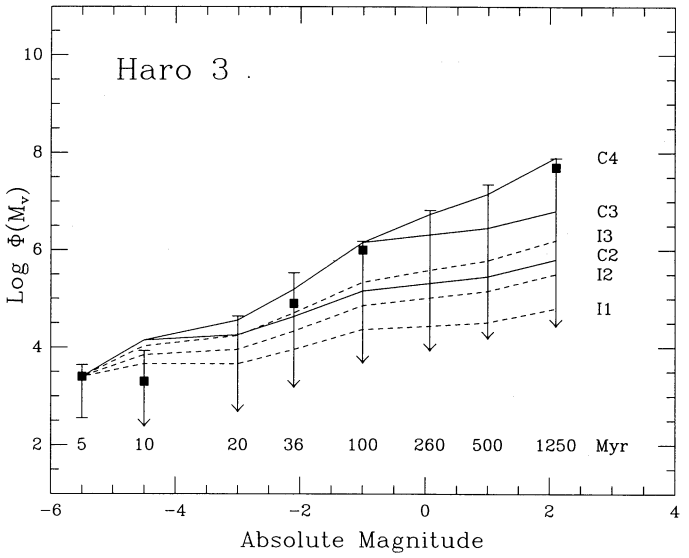

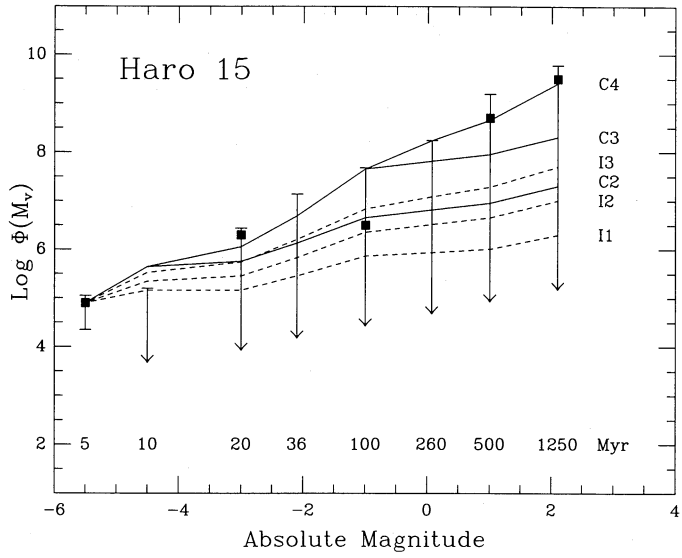

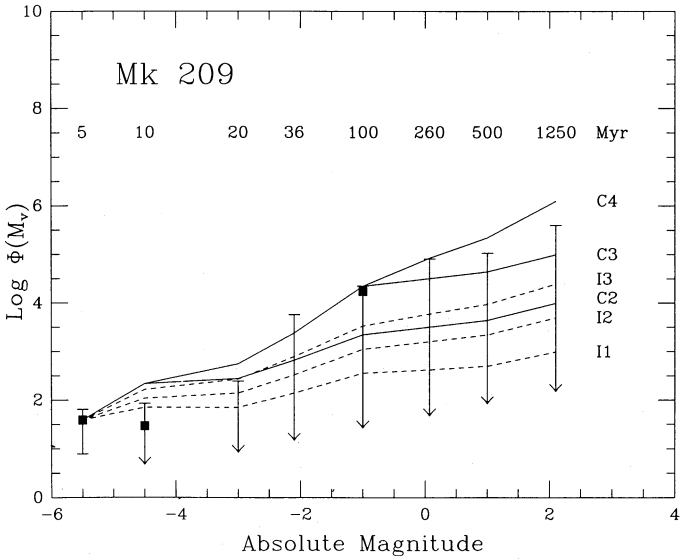

FIG. 5.—Main-sequence luminosity functions derived from the synthesis compared with those determined for simple evolutionary star formation histories. The eight stellar groups from O3–O6 V to A5–A7 V described in Paper I define the main sequence. Their lifetimes are indicated in Myr. Filled squares are the luminosity functions taken from the optimal unconstrained solutions. The 3 σ limits associated with each value are plotted. Their interpretation is described in the text. For those stellar groups not present in the unconstrained solutions, upper limits are displayed. Luminosity functions for several simple star formation histories, described in Table 9, are superposed onto the synthesis-derived luminosity functions: solid lines represent continuous star formation (CSF) models, and dashed lines are infinitely short burst (ISB) models.

of metal-poor OB I's, replaced in the unconstrained solution by main-sequence stars because they lack the rich ultraviolet line spectra of solar-metallicity blue supergiants. In this case, the number of B4–B7 stars would be overestimated, since one B supergiant is ~ 100 times more luminous at 1510 Å than a B4–B7 dwarf. The relative strength of the first three groups suggests that an ISB model with $x \lesssim 1.5$ is consistent with the data. This interpretation is consistent with VT83, based on optical spectrophotometry, and the result of applying constraint E1 (see above).

Although they are usually not well determined from the far-UV data, we believe that the A star components in our solutions point to significant star formation activity in the BCGs $\gtrsim 500$ Myr ago. The pre–main-sequence contraction time scale for these stars is long compared with that for the ionizing stars. Stars with $m = 2\ M_\odot$ ($\sim$A5) reach the main sequence in $\tau \approx 7$ Myr (Iben 1965; Stahler 1985), which occurs *after* the most massive stars of the current generation have died. Most of the A stars formed in the current burst are probably not yet visible, especially if they are still surrounded by their parental gas and dust envelopes. However, the results of imposing constraint type B demonstrate that the A star component is not spurious. Therefore, a detectable A star component in our models probably originates in *previous* star formation episodes. The A star components are not likely to represent a supergiant population because (1) the B8–A0 I group is not selected in the unconstrained solutions and (2) star counts in our Galaxy and the Magellanic Clouds indicate that the luminosity function of A supergiants is much smaller than for either OB or KM supergiants (e.g., Meylan and Maeder 1982). Massive stars evolve quickly through this temperature range in both directions, and therefore a major A supergiant component would imply a very peculiar stellar population present in nearly all our objects. The main-sequence A stars will produce strong Balmer absorption lines, which in fact are seen in IIDS spectra of Haro 1 and Haro 2 (Thuan 1981). We will study the A–F population further in Fanelli (1988), based on mid-UV (1900–3200 Å) *IUE* data.

To summarize: the best evidence is that the current burst of star formation in most of these BCGs has had a duration of less than 10 Myr. All objects, except perhaps Mrk 209, exhibit evidence of earlier star formation episodes. Data for Haro 2 indicate several earlier discrete bursts, but in the other cases we cannot distinguish between a few isolated bursts and a continuing series of short bursts separated by $\sim$20–30 Myr throughout the last ~ 1 Gyr.

IX. POST–MAIN-SEQUENCE POPULATIONS

Evolved OB stars are expected to be present in star-forming regions if the star formation started more than $\sim$3–5 Myr prior to the current epoch. In the infinitely short burst scenario, the initial population mix contains only main-sequence stars. As the population evolves, the most massive remaining stars will pass through the blue giant and supergiant stage, perhaps more than once (see § II). The fractional contribution of this evolved component depends on the details of massive star evolution and the initial mass function and is a strong function of time. In the continuous star formation scenario, an equilibrium population will be established, $n_j \propto t_j$, where t_j is the lifetime of each phase, if the time scale for star formation is much longer than the main-sequence lifetimes of the progenitors (O to mid-B spectral types) and if the amplitude of the star formation rate does not vary greatly.

Most of the BCGs studied here do not have a significant post–main-sequence population. Only in Haro 1 is a substantial blue supergiant component indicated (64% of the light at 1510 Å). Two spectral diagnostics of blue supergiants are a strong Si IV line (Walborn and Panek 1984; Paper I) and a feature centered at $\sim$1620 Å. Both features are present in Haro 1. On the other hand, there is little evidence for main-sequence types earlier than $\sim$O9. Table 6 shows that the O3–O6 V group contributes less than 5% of the light at all UV wavelengths (which constitutes only a marginal detection; cf. § IV*e*), while the O7–B0 V group is not selected. Thus, the progenitors of the dominant O9–B0 I component, O3–O9 dwarfs, are largely absent. This result points toward a burst model in which Haro 1 is now moving into a "postburst" phase. Barring a new episode of massive star formation, Haro 1 will, in $\sim$20–30 Myr, still display an excess blue flux compared with a normal spiral galaxy, but with a turnoff at $\sim$B4 and with no nebular emission lines.

No OB supergiants were selected in the unconstrained solution for Mrk 209; however, we do suspect the presence of some Wolf-Rayet stars. As discussed in Paper I, W-R stars are identified primarily by their characteristic emission lines. Since emission lines are difficult to detect against the strong UV continuum in star-forming regions, the presence of W-R stars in extragalactic H II regions is usually determined in the optical (Osterbrock and Cohen 1982; Kunth and Schild 1986). An optical spectrum of Mrk 209 presented by VT83 does show W-R features. The *IUE* spectrum exhibits a strong C III λ1909 emission line as well as weaker lines of N IV] λ1486, C IV λ1550, and [O III] λ1663. These lines may arise from both the ionized interstellar medium in Mrk 209 and the atmospheres of W-R stars. We note that abundances derived from such ultraviolet emission lines, especially of carbon (which does not have prominent optical emission lines), may not be indicative of general interstellar abundances if the lines have a strong circumstellar component. The abundance pattern in the atmospheres of W-R stars arises from material recently synthesized and does not reflect the metallicity of the gas from which the stars condensed.

X. IONIZING STELLAR POPULATIONS AND STAR FORMATION RATES

One advantage of ultraviolet population synthesis is the opportunity to measure directly the young, massive star population. Stars earlier than $\sim$B2 produce significant numbers of photons with $\lambda < 912$ capable of ionizing interstellar hydrogen. These photons produce a distinctive observational signature at optical, infrared, and radio wavelengths. In fact, the properties of young stellar populations have to date been estimated largely from the strong optical/infrared nebular emission lines which are produced by the material ionized by those stars. UV synthesis provides an *independent* method of estimating the ionizing photon luminosity and the massive star formation rate, which can be compared with that derived from Balmer emission lines or thermal radio continuum fluxes.

We have calculated the ionizing photon rate, $N_{\rm ion}$, the flux of Hα, I(Hα), and the thermal radio continuum flux, $S_{6\ \rm cm}$, for our models. The total stellar population present within the *IUE* aperture is found by scaling the normalized model flux to the observed flux using the distances listed in Table 1 and the optimal color excess. $N_{\rm ion}$ is calculated as $\sum N_{{\rm ion},i} n_i$, where n_i is the number of stars in group i, and $N_{{\rm ion},i}$ is the ionizing photon rate assigned to group i (described in Paper I) summed

over all groups present in a model. Assuming a standard nebular model (Osterbrock 1974), $I(\mathrm{H}\alpha)$ and $S_{6\ \mathrm{cm}}$ are derived following Lequeux (1980):

$$\frac{S_\nu}{1\ \mathrm{Jy}} = 1.33 \times 10^{-47} N_{\mathrm{ion}} \left(\frac{\nu}{1\ \mathrm{GHz}}\right)^{-0.1} \times \left(\frac{T_e}{10^4\ \mathrm{K}}\right)^{0.45} \left(\frac{D}{1\ \mathrm{kpc}}\right)^{-2}, \quad (8)$$

$$\frac{I(\mathrm{H}\alpha)}{\mathrm{ergs\ cm^{-2}\ s^{-1}}} = 1.16 \times 10^{-56} N_{\mathrm{ion}} \left(\frac{T_e}{10\ \mathrm{K}}\right)^{0.09} \left(\frac{\mathrm{D}}{1\ \mathrm{kpc}}\right)^{-2}, \quad (9)$$

where S_ν is the continuum flux at frequency ν, T_e is the nebular electron temperature, and D is the distance in kiloparsecs. We assume an electron temperature of 10,000 K for Haro 1, 2, 3, and 15. VT83 give $T_e \approx 14{,}500$ K for Mrk 209; Tully *et al.* (1981) find $T_e \approx 15{,}000$ K for VII Zw 403. We note that these relations assume that no ionizing photons are destroyed by dust. Within the limitations imposed by the variety of apertures and calibrations employed, we can compare these quantities with independent observations taken from the literature and our own unpublished data. In Table 8 we give the model predictions and available data. We list $F(\mathrm{H}\alpha)$, the *extincted* Hα flux, determined from the value of $I(\mathrm{H}\alpha)$ computed above, the synthesis-derived color excess, and the Savage and Mathis (1979) reddening law (f_λ); $F(\mathrm{H}\alpha) = I(\mathrm{H}\alpha) \times 10^{-0.4 f_{\mathrm{H}\alpha} E(B-V)}$.

The ratios of calculated to observed radio fluxes are found to be in the range 0.36–0.72. The ionizing population derived by the synthesis thus produces ~50% of the observed signal at 6 cm, with a weak tendency for the less luminous objects to have a larger ratio of calculated to observed radio flux. Since most of the data are single-dish observations taken with a beam size (2.'46) much larger than the *IUE* spectrograph aperture, the additional radio flux could arise outside this area or from a population of supernova remnants. Klein, Wielebinski, and Thuan (1984) find a mean radio index for 14 BCGs $\langle\alpha\rangle \approx -0.33$ ($S_\nu \propto \nu^\alpha$), indicating that both a thermal and a nonthermal component are present in that sample. In Mrk 209, for which VT83 provide a 6 cm radio map, $S_{6\ \mathrm{cm}}$(predicted) ≈ $S_{6\ \mathrm{cm}}$(observed) and agrees with their conclusion that the radio flux from this source has a thermal origin.

The ratios of predicted to observed radio flux imply that the synthesis technique gives an accurate measure of N_{ion} and of the extinction affecting the star-forming regions. Larger values of $E(B-V)$ would produce a larger ionizing star population and increased 6 cm flux, exceeding the observed values. Additionally, there cannot be extensive amounts of "hidden" star formation—i.e., obscured regions which would still produce significant 6 cm flux (which is unaffected by dust). The assumption that dust does not compete strongly for the ionizing photons appears justified. The data for Mrk 209 demonstrates that full utilization of the radio continuum flux as a diagnostic for the ionizing star population requires multifrequency radio maps, where thermal and nonthermal components can be identified and evaluated for any specified aperture.

Predicted and observed values of the Balmer line flux are in reasonable agreement, given the aperture differences, for Haro 3, Mrk 209, and VII Zw 403, the only BCGs with available data. Interestingly, in Mrk 209 the ultraviolet and optical data give a similar value for the intrinsic ionizing photon rate, even though the extinctions determined from the UV synthesis and the Balmer line ratios are different. Similarly, the Hα flux predicted by the model agrees with the data for VII Zw 403 (Tully *et al.* 1981) despite a similar difference in the estimated extinction. Observations in these two wavelength ranges are in agreement on the ionizing stellar population even though the emergent SED sppears to experience nonuniform extinction.

We can also derive a lower limit on the massive star formation rate, $\dot{M}$. In Table 6 we give these results derived by dividing the number of stars with $m \geq 10\ M_\odot$ given in Table 6 by their respective lifetimes (Table 2 in Paper I) to produce a time-averaged star formation rate. This procedure ignores variations in $\dot{M}$ on shorter time scales. We also calculate $\dot{M}$ for stars with $m > 2\ M_\odot$, the approximate limiting stellar mass for production of significant flux in the far-UV bandpass, according to equation (4) normalized to the massive ($m > 10\ M_\odot$) star formation rate and taking $x = 1.8$. The expected supernova rate (SNR), assuming that all stars with $m > 10\ M_\odot$ become supernovae, is also listed in Table 6.

The formation rate of *massive* ($m \geq 10\ M_\odot$) stars ranges from $3 \times 10^{-4}\ M_\odot\ \mathrm{yr}^{-1}$ for the low-luminosity dwarf Mrk 209 to $\sim 3\ M_\odot\ \mathrm{yr}^{-1}$ for the most luminous BCGs, Haro 1 and Haro 15, where tens of thousands of O stars are observed. For the latter BCGs, a burst lasting 5 Myr will process a total of $1.5 \times 10^7\ M_\odot$ of gas through stars in this mass range alone, and $\sim 10^8\ M_\odot$ of gas through stars with $m > 2\ M_\odot$. The UV synthesis clearly indicates that intense star formation episodes are occurring in these BCGs measured by the *observed* massive star population. Since far-ultraviolet data contain no information on the production rate of cooler stars, we cannot directly measure "total" star formation rates, but we note that for normal IMFs very high rates would be implied [$\dot{M}_{\mathrm{tot}}(100 > m/M_\odot > 0.1) \approx 8\ \dot{M}(100 > m/M_\odot > 10)$ for a Salpeter IMF].

Two of our galaxies, Haro 2 and Haro 3, were studied by Thronson and Telesco (1986), who estimated star formation rates from *IRAS* data. Using their calibration and values for L_{IR}, $\dot{M}_{\mathrm{IR}}$(OBA) is equal to $0.84\ M_\odot\ \mathrm{yr}^{-1}$ for Haro 2 and $0.42\ M_\odot\ \mathrm{yr}^{-1}$ for Haro 3. Even though the *IRAS* data refer to the entire galaxy, the SFR derived from far-IR data for OBA stars is in excellent agreement with the rate derived for $m > 2\ M_\odot$ for Haro 2, and ~3 times larger for Haro 3. *IRAS* and *IUE* are therefore observing the same star-forming region in Haro 2, a conclusion strengthened by the UV light profile presented in Figure 2, which indicates that the star formation region is contained within the smaller *IUE* aperture.

We have found that the rates of massive star formation in the BCGs estimated independently from UV spectral synthesis, optical emission lines, the radio continuum, and far-infrared emission are very similar, perhaps surprisingly so. This increases one's confidence in any of these methods used alone. Star formation rates derived from ultraviolet spectra do not depend on uncertainties concerning the source of the luminosity (dust-obscured active nucleus, reradiated shock energy) which may affect those determined from far-IR (*IRAS*) data.

The strength of the star formation in these BCGs adds weight to the starburst concept. We intend to consider the implications of these results concerning the history of BCG star formation for the classic problems of gas consumption, metal enrichment, and the statistics of BCG colors, but we postpone this to a later paper.

XI. SUMMARY

We have investigated the stellar content of seven blue compact galaxies quantitatively by applying the technique of

optimizing population synthesis to far-UV spectra taken with the *IUE* satellite. We reach the following conclusions:

1. The rich far-UV line spectra of hot stars and the negligible contribution of cool stars to the integrated far-UV light provide excellent diagnostics for investigating the nature of the hot population in star-forming regions. The far-UV spectra of BCGs clearly indicate a composite population with spectral types between O3 and mid-A. P Cygni profiles for Si IV and C IV are observed in several objects.

2. Our linear programming synthesis technique is capable of giving excellent fits to the observed far-UV spectra. In the best cases, the quality of the fit (residuals smaller than 4% per 20 Å bandpass) appears to be governed by the observational error in the galaxy spectra rather than deficiencies in the stellar library used or uncertainties in the extinction.

3. Unconstrained synthesis models (Table 6) yield stellar luminosity functions exhibiting sharp discontinuities, which indicates a star formation history characterized by discrete star formation episodes or bursts. We have examined the reality of these discontinuities using a variety of constrained models (cf. Tables 5 and 7 and Fig. 5) and conclude that continuous star formation ($\dot{M} \sim$ constant for $\gtrsim 100$ Myr) cannot account for the observations. Neither can a single short burst of star formation, except possibly in the case of Mrk 209, a metal-poor blue compact dwarf. The current burst of star formation in most objects appears to have lasted for less than 10 Myr. For Haro 2, synthesis indicates at least two earlier bursts of larger amplitude, the most recent of which ended not more than ~ 20 Myr ago. A stars in our models, although they are not usually well constrained by the far-UV data, point to significant star formation activity in most of these BCGs $\gtrsim 500$ Myr ago. In the cases other than Haro 2, we cannot distinguish between a few isolated bursts or a continuing series of short bursts separated by ~ 20–30 Myr throughout the last ~ 1 Gyr.

4. Except for Haro 1, none of these objects appears to possess a significant population of blue supergiants. In Haro 1, O9–B0 I stars produce 52% of the light at 1510 Å, and their number, relative to the O3–O6 V population, provides additional evidence for a recently ended burst of star formation. The massive O V stars formed ~ 3–5 Myr ago have now evolved into a supergiant phase.

5. UV synthesis provides an independent estimate of the current ionizing star content which appears to be in agreement with estimates based on Balmer line emission or thermal radio continuum methods.

6. A reliable measure of the extinction affecting the UV continuum is provided by the synthesis technique. The amount of UV extinction is found to be low in the observed BCGs, corresponding to $E(B-V) \sim 0.0$–0.35. It is usually significantly lower than values derived from the Balmer decrement for the same object, indicating that the UV light preferentially emerges through windows of low optical depth. The dust in the star-forming regions has probably been destroyed through the combined action of ionizing radiation, stellar winds, and supernovae. There appears to be a positive correlation between the amount of UV extinction and the metallicity of the galaxy.

7. Most of the absorption lines present in the UV spectra appear to have a stellar origin, including the low-ionization lines often assumed to arise in the interstellar medium. The blue compact dwarf, Mrk 209, displays weak absorption lines which cannot be matched by our solar-metallicity library. This is evidence that the stellar component has the same low metallicity as observed in the ionized gas ($Z \sim 0.1\ Z_\odot$).

8. The intensity of the starbursts observed in the more luminous objects here is striking. Approximately 3 $M_\odot\ \mathrm{yr}^{-1}$ of gas is being converted into the observed massive ($m \gtrsim 10\ M_\odot$) star population in Haro 1 and Haro 15. For an IMF with a slope $x = 1.8$, the estimated star formation rate for $m \gtrsim 2\ M_\odot$ ranges from $0.002\ M_\odot\ \mathrm{yr}^{-1}$ for the low-luminosity dwarf Mrk 209 to $\sim 15\ M_\odot\ \mathrm{yr}^{-1}$ for the luminous BCGs Haro 1 and Haro 15. When star formation in the current starburst ends, the ionizing stars will complete their evolution in ~ 20 Myr. Subsequently, during the interburst period, the spectral energy distribution will continue to exhibit the strong blue continuum produced by the later B and A stars formed in the burst but will lack the characteristic emission lines seen in actively star-forming galaxies.

This work has been supported in part by National Aeronautics and Space Administration grants NAG 5-700 and 5-838 (R. W. O. and M. N. F.) and by NAG 5-257 (T. X. T. and M. N. F.). T. X. T. acknowledges partial financial support from a Fulbright fellowship and is grateful for the hospitality of the Institut d'Astrophysique de Paris and the Service d'Astrophysique at the Center d'Etudes Nucléaires de Saclay in France.

REFERENCES

Balzano, V. A. 1983, *Ap. J.*, **268**, 602.
Benvenuti, P., Casini, C., and Heidmann, J. 1979, *Nature*, **282**, 272.
———. 1982*a*, *M.N.R.A.S.*, **198**, 825.
———. 1982*b*, in *Advances in Ultraviolet Astronomy: Four Years of IUE Research*, ed. Y. Kondo (Greenbelt: NASA/Goddard Space Flight Center), p. 156.
Bergvall, N. 1985, *Astr. Ap.*, **146**, 269.
Bertelli, G., Bressan, A. G., and Chiosi, C. 1984, *Astr. Ap.*, **130**, 279.
Böhm-Vitense, E., Hodge, P., and Boggs, D. 1984, *Ap. J.*, **287**, 825.
Bohlin, R. C., Hill, J. K., Stecher, T. P., and Witt, A. A. 1982, *Ap. J.*, **255**, 87.
Bohlin, R. C., and Holm, A. V. 1980, *NASA IUE Newsletter*, No. 10, p. 37.
Bohlin, R. C., Holm, A. V., Savage, B. D., Snijders, M. A., and Sparks, W. M. 1980, *Astr. Ap.*, **85**, 1.
Brunish, W. M., and Truran, J. W. 1982*a*, *Ap. J.*, **256**, 247.
———. 1982*b* *Ap. J. Suppl.*, **49**, 447.
Burenkov, A. N., and Khachikyan, E. E. 1986, *Astrofizkia*, **24**, 349.
Burstein, D. 1985, *Pub. A.S.P.*, **97**, 89.
Cassatella, A., Barbero, J., and Benvenuti, P. 1983, in *ESA IUE Newsletter*, No. 18, p. 38.
Chiosi, C. 1982, in *IAU Symposium 99, Wolf-Rayet Stars: Observations, Physics, Evolution* (Dordrecht: Reidel), p. 323.
Chiosi, C., and Maeder, A. 1986, *Ann. Rev. Astr. Ap.*, **24**, 329.
Clayton, D. E. 1968, *Principles of Stellar Evolution and Nucleosynthesis* (New York: McGraw-Hill).
Conti, P. S., Garmany, C. D., de Loore, C., and Vanbeveren, D. 1983, *Ap. J.*, **274**, 302.
de Vaucouleurs, G., de Vaucouleurs, A., and Corwin, H. G. 1976, *Second Reference Catalogue of Bright Galaxies* (Austin: University of Texas Press) (RC2).
Doom, C. 1982, *Astr. Ap.*, **116**, 303.
Dufour, R. J., Shields, G. A., and Talbot, R. J. 1982, *Ap. J.*, **252**, 461.
Fabbiano, G., and Panagia, N. 1983, *Ap. J.*, **266**, 568.
Fanelli, M. N. 1988, in preparation.
Fanelli, M. N., O'Connell, R. W., and Thuan, T. X. 1987, *Ap. J.*, **321**, 768 (Paper I).
French, H. B. 1980, *Ap. J.*, **240**, 41.
Garmany, C. D., and Conti, P. S. 1985, *Ap. J.*, **293**, 407.
Garmany, C. D., Olson, G. L., Conti, P. S., and Van Steenberg, M. E. 1981, *Ap. J.*, **250**, 660.
Gehrz, R. D., Sramek, R. A., and Weedman, D. W. 1983, *Ap. J.*, **267**, 551.
Gordon, D., and Gottesman, S. T. 1981, *A.J.*, **86**, 161.
Haro, G. 1956, *Bol. Obs. Tonantzintla y Tacubaya*, **14**, 8.
Heiles, C. 1975, *Astr. Ap. Suppl.*, **20**, 37.
Huchra, J. P. 1977*a*, *Ap. J.*, **217**, 928.
———. 1977*b*, *Ap. J. Suppl.*, **35**, 171.
Huchra, J. P., Geller, M. J., Gallagher, J., Hunter, D., Hartmann, L., Fabbiano, G., and Aaronson, M. 1983, *Ap. J.*, **274**, 125.
Humphreys, R. M., and McElroy, D. B. 1984, *Ap. J.*, **284**, 565.

Humphreys, R. M., Nichols, M., and Massey, P. 1985, *A.J.*, **90**, 101.
Hunter, D. A. 1982, *Ap. J.*, **260**, 81.
Hunter, D. A., Gallagher, J. S., and Rautenkranz, D. 1982, *Ap. J.*, **49**, 53.
Hutchings, J. B. 1982, *Ap. J.*, **255**, 70.
Iben, I. 1965, *Ap. J.*, **141**, 993.
———. 1967, *Ann. Rev. Astr. Ap.*, **5**, 571.
Israel, F. P., and Koornneef, J. 1979, *Ap. J.*, **230**, 390.
Kinman, T. D., and Davidson, K. 1981, *Ap. J.*, **243**, 127.
Klein, U., Wielebinski, R., and Thuan, T. X. 1984, *Astr. Ap.*, **141**, 241.
Kunth, D., and Sargent, W. L. 1983, *Ap. J.*, **273**, 81.
Kunth, D., and Schild, H. 1986, *Astr. Ap.*, **169**, 71.
Kunth, D. and Sevre, F. 1986, in *Star-forming Dwarf Galaxies and Related Objects*, ed. D. Kunth, T. X. Thuan, and J. T. T. Van (Gif-sur-Yvettes: Editions Frontières), p. 331.
Lamb, S. A., Gallagher, J. S., Hjellming, M. S., and Hunter, D. A. 1985, *Ap. J.*, **291**, 63.
Lequeux, J. 1980, in *Star Formation* (Saas-Fée: Geneva Observatory), p. 99.
Lequeux, J., Maucherat-Joubert, M., Deharveng, J. M., and Kunth, D. 1981, *Astr. Ap.*, **103**, 305.
Lequeux, J., Peimbert, M., Rayo, J. F., Serrano, A., and Torres-Peimbert, S. 1979, *Astr. Ap.*, **80**, 155.
Longo, G., and de Vaucouleurs, A. 1983, *A General Catalog of Photoelectric Magnitudes and Colors in the UBV System* (Austin: University of Texas).
Loose, H-H., and Thuan, T. X. 1986, in *Star-forming Dwarf Galaxies and Related Objects*, ed. D. Kunth, T. X. Thuan and J. T. T. Van (Gif-sur-Yvette: Editions Frontières), p. 73.
Maeder, A. 1984, in *IAU Symposium 105, Observational Tests of the Stellar Evolution Theory* (Dordrecht: Reidel), p. 299.
Markarian, B. E. 1967, *Astrofizika*, **3**, 55.
Massa, D., and Fitpatrick, E. L. 1986, *Ap. J. Suppl.*, **60**, 305.
Massa, D., and Savage, B. D. 1985, *Ap. J.*, **299**, 905.
Massa, D., Savage, B. D., and Fitzpatrick, E. L. 1983, *Ap. J.*, **266**, 662.
Massey, P., and Conti, P. S. 1983, *Ap. J.*, **273**, 576.
Matteucci, F., and Chiosi, C. 1983, *Astr. Ap.*, **123**, 121.
Meylan, G., and Maeder, A. 1982, *Astr. Ap.*, **108**, 148.
Nandy, K., Morgan, D. H., Willis, A. J., Wilson, R., Gondhalekar, P. M., and Houziaux, L. 1980, *Nature*, **283**, 725.
O'Connell, R. W. 1973, *A.J.*, **78**, 1074.
———. 1976, *Ap. J.*, **206**, 370.
———. 1980, *Ap. J.*, **236**, 430.
———. 1983, *Ap. J.*, **267**, 80.
O'Connell, R. W., Thuan, T. X., and Goldstein, S. J. 1978, *Ap. J. (Letters)*, **266**, L11.
Osterbrock, D. E. 1974, *Astrophysics of Gaseous Nebulae* (San Francisco: Freeman).
Osterbrock, D. E., and Cohen, R. D. 1982, *Ap. J.*, **261**, 64.
Rocca- Volmerange, B., Prévot, L., Ferlet, R., Lequeux, J., and Prévot-Burnichon, M. L. 1981, *Astr. Ap.*, **99**, L5.
Rosa, M., Joubert, M., and Benvenuti, P. 1984, *Astr. Ap. Suppl.*, **57**, 361.
Savage, B. D., and Mathis, J. S. 1979, *Ann. Rev. Astr. Ap.*, **17**, 73.
Scalo, J. M. 1986, in *Fund. Cosmic Phys.*, **11**, 1.
Searle, L., and Sargent, W. L. 1972, *Ap. J.*, **173**, 25.
Searle, L., Sargent, W. L., and Bagnuolo, W. G. 1973, *Ap. J.*, **179**, 427.
Stahler, S. W. 1985, *Ap. J.*, **293**, 207.
Stasinska, G. 1982, *Astr. Ap. Suppl.*, **48**, 299.
Stothers, R., and Chin, C.-W. 1976, *Ap. J.*, **204**, 472.
Thronson, H. A., and Telesco, C. M. 1986, *Ap. J.*, **311**, 98.
Thuan, T. X. 1981, private communication.
———. 1986, in *Star-forming Dwarf Galaxies and Related Objects*, ed. D. Kunth, T. X. Thuan, and J. T. T. Van (Gif-sur-Yvette: Editions Frontières), p. 105.
———. 1988, in *Starbursts and Galaxy Evolution*, ed. T. X. Thuan, T. Montmerle, and J. T. T. Van (Gif-sur-Yvette: Editions Frontières), p. 129.
Thuan, T. X., and Condon, J. J. 1987, *Ap. J. (Letters)*, **322**, L9.
Thuan, T. X., and Martin, G. 1981, *Ap. J.*, **247**, 823.
Thuan, T. X., Montmerle, T., and Van, J. T. T. 1988, *Starbursts and Galaxy Evolution* (Gif-sur-Yvette: Deditions Frontières).
Tinsley, B. M. 1980, *Fund. Cosmic Phys.*, **5**, 287.
Tully, R. B., Boesgaard, A. M., Dyck, H. M., and Schempp, W. V. 1981, *Ap. J.*, **146**, 38.
Turnrose, B. E. 1976, *Ap. J.*, **210**, 33.
Turnrose, B. E., and Thompson, R. W. 1984, *IUE Image Processing Information Manual* (Greenbelt: NASA/Goddard Space Flight Center).
Viallefond, F., and Thuan, T. X. 1983, *Ap. J.*, **269**, 444 (VT83).
Walborn, N. R., and Panek, R. J. 1984, *Ap. J. (Letters)*, **280**, L27.
Weedman, D. W., Feldman, F. R., Balzano, V. A., Ramsey, L. W., Sramek, R. A., and Wu, C.-C. 1981, *Ap. J.*, **248**, 105.
West, R. M., Lauberts, A., and Schuster, H. E. 1987, *IAU Circ.*, No. 4356.
Witt, A. N., Bohlin, R. C., and Stecher, T. P. 1984, *Ap. J.*, **279**, 698.
Wu, C.-C., *et al.* 1983, *The IUE Ultraviolet Spectral Atlas* (Greenbelt: NASA/Goddard Space Flight Center).
Zwicky, F., and Zwicky, M. A. 1971, *Catalogue of Selected Compact Galaxies and of Post-eruptive Galaxies* (Guemligen, Switzerland: F. Zwicky).

MICHAEL N. FANELLI, ROBERT W. O.'CONNELL, and TRINH X. THUAN: Astronomy Department, University of Virginia, Charlottesville, VA 22903-0818